NJC

ROYAL SOCIETY OF CHEMISTRY

PAPER

View Article Online
View Journal | View Issue

Cite this: *New J. Chem.*, 2025, **49**, 12688

Synthesis and biological studies on ovarian cancer cells of new heterocyclic molecules inspired by MIM1, an inhibitor of the anti-apoptotic protein Mcl-1†

Jocelyn Pezeril, ‡[ab] Louis-Bastien Weiswald,‡[ab] Ali Soulieman,‡[cd] Hippolyte Paysant,[ab] Ali Hachem,[d] Emilie Brotin,[abe] Christophe Denoyelle,[abe] Anne-Sophie Voisin-Chiret,[f] Nicolas Gouault,[c] René Grée,*[c] Nicolas Levoin*[g] and Laurent Poulain*[ab]

Received 13th January 2025,
Accepted 15th June 2025

DOI: 10.1039/d5nj00175g

rsc.li/njc

Research on new and potent inhibitors of anti-apoptotic proteins is a very active and promising topic in bioorganic and medicinal chemistry. MIM1 is a small molecule that was among the first reported inhibitors of the anti-apoptotic protein Mcl-1. We recently corrected its structure and developed a focused library of analogues to obtain new dual Bcl-x_L/Mcl-1 inhibitors as well as selective Mcl-1 inhibitors. All the corresponding molecules contained a triphenol core, established by molecular modelling as the key component to anchor these products to the binding site of these proteins. Thus, as a next step, we designed and synthesized novel analogues in which this labile core was replaced by a *meta* carboxylic acid. A focused library of such molecules was submitted to a set of *in cellulo* biological studies, which allowed new potent and selective inhibitors of Mcl-1 to be identified. Preliminary structure–activity relationships were elucidated, and molecular modelling studies allowed us to propose a rationale for the biological activity of this series of new inhibitors, in particular for the inhibition of the anti-apoptotic protein Mcl-1.

Introduction

Cell death escape, a hallmark of cancer, is involved in carcinogenesis and chemoresistance[1] and is frequently due to the deregulation of apoptosis and particularly through perturbations in the control of the intrinsic pathway, which is itself in part governed by the Bcl-2 family.[2]

Bcl-2 family proteins are classified according to the presence of one or more Bcl-2 homology (BH) domains (BH1–BH4) and their pro- or anti-apoptotic activity. Anti-apoptotic proteins that possess BH1 to BH4 domains (Bcl-2, Bcl-x_L, Mcl-1, Bcl-w, A1 and Bfl-1) are capable of sequestering pro-apoptotic proteins in their hydrophobic pocket formed by BH1–BH3 domains and hindering their function. Pro-apoptotic proteins are subdivided into two groups: BH multi-domains (domains BH1–BH3), also known as "effectors" (Bax and Bak), and "BH3-only" proteins, possessing only the BH3 domain. BH3-only proteins are further divided into "activator" proteins (Bim, Bid, and Puma), activated in response to a cell-death signal and able to directly activate Bax and Bak, and "sensitizer" proteins (Noxa, Bad, Hrk, Bmf, Bik), which antagonize the function of anti-apoptotic proteins by interacting through the alpha-helix of their BH3 domain with the hydrophobic pocket of anti-apoptotic proteins. This interaction leads to the release of activator BH3-only proteins and/or multi-domain proteins as well as to subsequent mitochondrial membrane permeabilization and associated apoptotic cell death.[3]

Since it has been previously shown that anti-apoptotic Bcl-2 family proteins are overexpressed in human cancers[4] and frequently associated with resistance to anti-cancer therapies,[5]

[a] *Université de Caen Normandie, Inserm U1086 ANTICIPE "Unité de Recherche Interdisciplinaire pour la Prévention et le Traitement des Cancers", Caen, France*
[b] *UNICANCER, Comprehensive Cancer Centre François Baclesse, Caen, France*
[c] *Univ Rennes, CNRS, ISCR (Institut des Sciences Chimiques de Rennes, UMR 6226), F-35000 Rennes, France*
[d] *Laboratoire de Chimie Médicinale et de Produits Naturels, Université Libanaise, Faculté des Sciences et PRASE-EDST, Hadath, Beyrouth, Lebanon*
[e] *Université de Caen Normandie, Services unit PLATON, ImpedanCELL core facility, Caen, France*
[f] *Université de Caen Normandie, Normandie Univ., CERMN, Caen, France*
[g] *Bioprojet-Biotech, 4 rue du Chesnay Beauregard, BP 96205, 35762 Saint Grégoire, France*

† Electronic supplementary information (ESI) available: Copies of ^{1}H NMR and ^{13}C NMR spectra for compounds **11–24**. See DOI: https://doi.org/10.1039/d5nj00175g

‡ Equal contribution to this work.

the possibility to develop pro-apoptotic strategies has been intensively investigated. One of the first strategies employed was to mimic BH3-only proteins to inhibit the activity of the anti-apoptotic proteins of the Bcl-2 family. It was firstly shown that the inhibition of the expression or activity of these proteins can induce apoptosis.[6–9] Thus, studies focused on these targets allowed for the identification of selective pharmacological inhibitors of Bcl-2, Bcl-x_L or Mcl-1.[10] Multiple preclinical studies showed that they could be interestingly combined together,[11–15] with conventional chemotherapeutic agents[16,17] or targeted therapies[18–24] in various cancers. All these conclusive preclinical studies led to multiple clinical trials with various BH3 mimetics and ultimately to the approval of VENCLEXTA® (ABT-199 or Venetoclax, targeting Bcl-2 protein) by the U.S Food and Drug Administration for treatment of patients with chronic lymphocytic leukemia and acute myeloid leukemia.[25]

However, it has also been shown that anti-apoptotic proteins could play a redundant role and that it could be required, in some cases, to inhibit concomitantly some of them to induce cancer cell death. For instance, it has been demonstrated that the expression of Mcl-1 could constitute one of the mechanisms of resistance to BH3-mimetic molecules targeting Bcl-2/Bcl-x_L proteins[26–29] and that Mcl-1 downregulation[30–32] or inhibition[11,33,34] could restore sensitivity to these BH3-mimetics.

Mcl-1 has been identified as a target of interest for the treatment of cancer because amplification of the MCL1 gene is one of the most common genetic changes observed in cancer[35] and overexpression of the Mcl-1 protein has been observed in both hematologic cancers[36] and solid tumors[37–40] including ovarian cancer.[41] Various Mcl-1 inhibitors have been developed by others following these findings.[42] Here, we focused our attention on derivatives of MIM1 (Mcl-1 inhibitor molecule 1), initially reported in 2012,[43] and which was described as able to displace a fluorescently labelled Mcl-1 SAHB$_A$ (stabilised α-helix of Bcl-2 domain) from the BH3-binding domain of Mcl-1 and not displace a fluorescently labelled Bad-BH3 peptide from the BH3-binding domain of Bcl-x_L. Despite a modest Mcl-1 inhibitor activity (IC_{50} = 4.8 μM), MIM1 was the first BH3-mimetic to show selectivity for Mcl-1 over Bcl-x_L.

We recently corrected the structure of MIM1 to **1** and prepared a series of MIM1 analogues **2**.[44] In a second step, we synthesised compound **3** (FJ809) with the structure originally assigned to MIM1 and demonstrated that this molecule exhibited physical, chemical and biological properties that differ from those of MIM1.[45] Most of the new analogues **2**, that we prepared, are more potent inhibitors than MIM1 and exhibit attractive properties either as selective inhibitors of Mcl-1 or dual inhibitors of Mcl-1 and Bcl-x_L.[44] However, all these compounds possess a triphenol structure, which is a key component to anchor onto the proteins, essentially with D256/R263 in the case of Mcl-1 and R139/D133 and/or R132/E129 in the case of Bcl-x_L. However, it is known that polyphenols are among the scaffolds related to frequent hitters of pan assay interference compounds (PAINS).[46] Therefore, it appeared of interest to us to design alternative molecules devoid of such a property, and preliminary molecular modelling studies indicated that

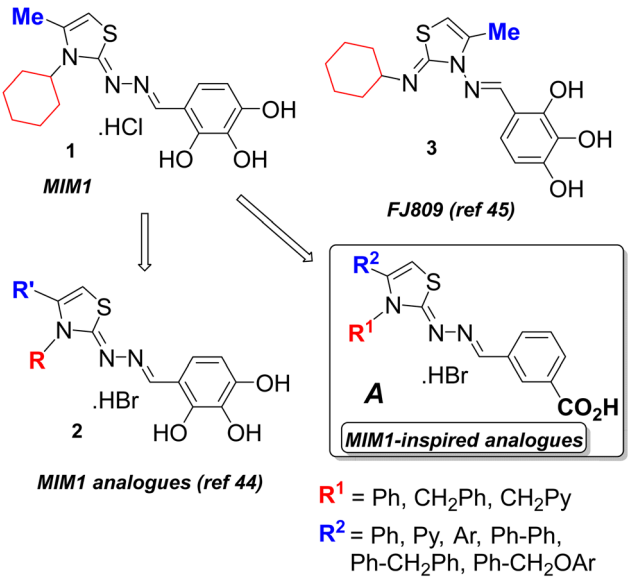

Fig. 1 Design of our targeted "MIM1-inspired" analogues.

including an acid in the *meta* position of an aromatic ring could be a good alternative to the triphenol moiety (Fig. 1, structure **A**). Further, in this design, the nature of the substituents $\mathbf{R^1}$ and $\mathbf{R^2}$ should offer attractive possibilities for the modulation of the properties of these "MIM1-inspired" molecules **A**.

We examined the pro-apoptotic activity of these molecules by appropriate biological studies, performed in the relevant ovarian cancer cell line model (IGROV1-R10), showing a dependence on both Bcl-x_L and Mcl-1 for their survival, thus allowing us to identify Bcl-x_L inhibitors, Mcl-1 inhibitors and dual inhibitors, as previously described.[44]

Therefore, the purpose of this paper is: (1) to describe the synthesis of selected examples of these target molecules **A**, (2) to report the results of their biological activity on the Mcl-1 and Bcl-x_L anti-apoptotic proteins using the same *in cellulo* procedures as used earlier for MIM1 and its analogues **2** and (3) to rationalize the structure–activity-relationship profiles of these new series of molecules through extensive molecular modelling studies.

Results

Chemical synthesis

The retrosynthetic analysis for our target molecules is indicated in Scheme 1.

The analogues **A** could be obtained by a cyclocondensation process between α-bromoketones and imino-thiosemicarbazides. Later derivatives are accessible through the reaction of *m*-carboxy benzaldehyde with thioureas. These intermediates are themselves prepared by reaction of the corresponding isothiocyanates with hydrazine hydrate. For our molecules, the molecular diversity is controlled first at the level of starting isocyanates (for $\mathbf{R^1}$) and in the final cyclocondensation step for $\mathbf{R^2}$.

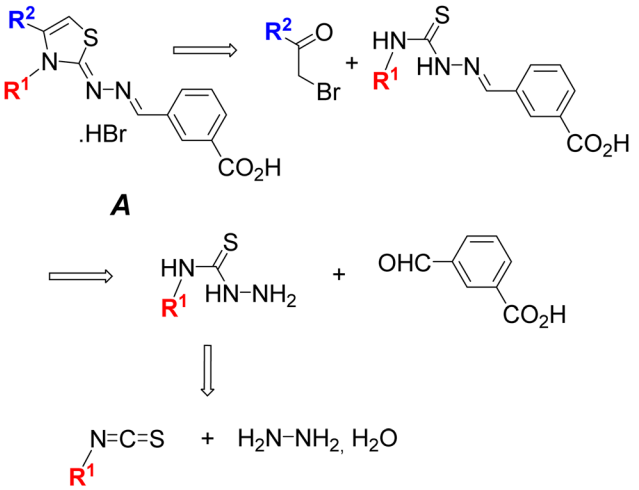

Scheme 1 Retrosynthetic analysis for the preparation of target molecules **A**.

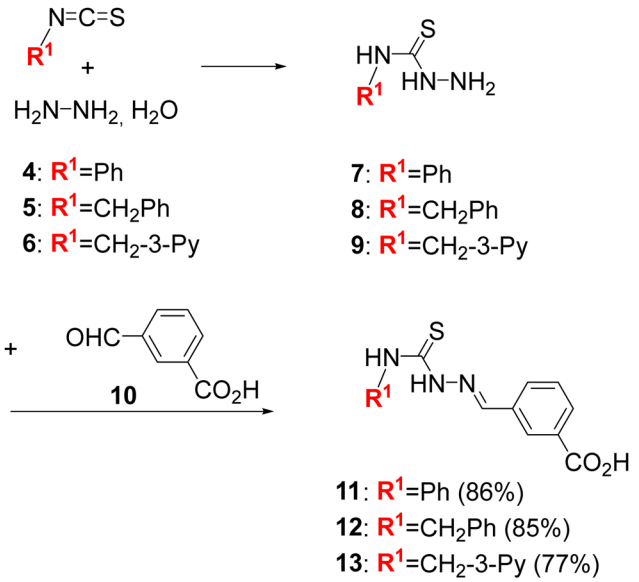

Scheme 2 Synthesis of intermediate thioureas and thiohydrazones.

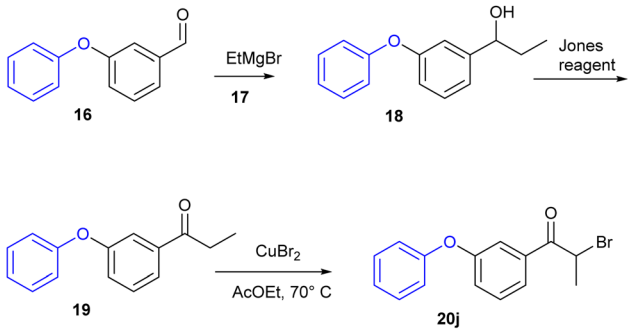

Scheme 4 Synthesis of acetyl bromide **20j**.

The synthesis of the thioureas **7–9** was performed by reaction of the known isocyanates **4–6** with hydrazine hydrate. Next, condensation of these thioureas **7–9** with aldehyde **10** gave the imino-thiosemicarbazides **11–13**, as indicated in Scheme 2. All these intermediates were obtained in excellent overall yields and characterized with respect to their physical and analytical properties (see the Experimental section and ESI†).

The second key components are the α-bromoketones. Most of them are commercially available (**15a–g**) but seven others (**15h–n**) were synthesized starting from the corresponding methylketones **14** *via* a bromination reaction according to Scheme 3.

Based on the first biological results, we also prepared one example of an acetylbromide with an extra methyl group in position 2: **20j**. The synthesis follows a three-step process from aldehyde **16**, as indicated in Scheme 4. Reaction with ethylmagnesium bromide **17**, afforded alcohol **18**, which was oxidized to the ketone **19** and finally, a bromination reaction gave the required intermediate **20j**.

The type-**A** target molecules were obtained by the condensation of the imino-semicarbazides **11–13** with the α-bromoketones **15** or **20j**, as indicated in Schemes 5 and 6. All these molecules were obtained in fair to excellent overall yields and characterized with respect to their physical and analytical properties (see the Experimental section and ESI†).

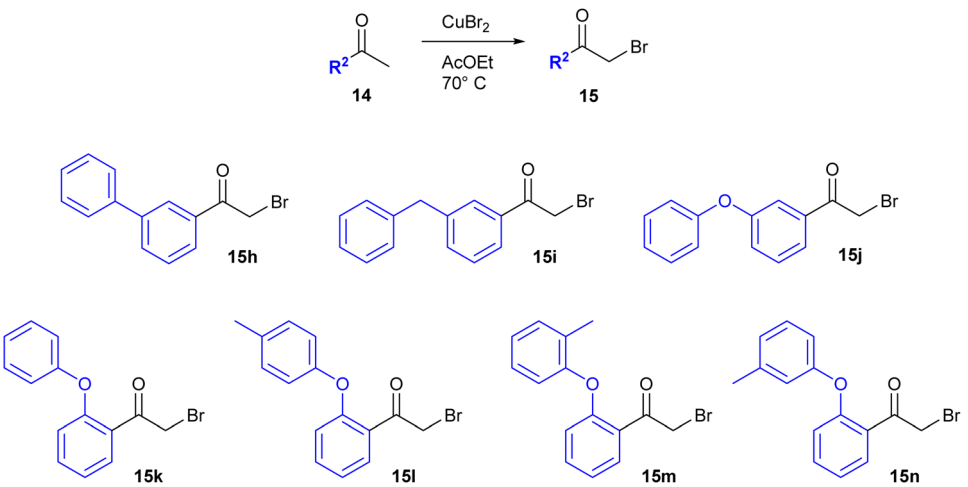

Scheme 3 Synthesis of α-bromoketones **15h–n**.

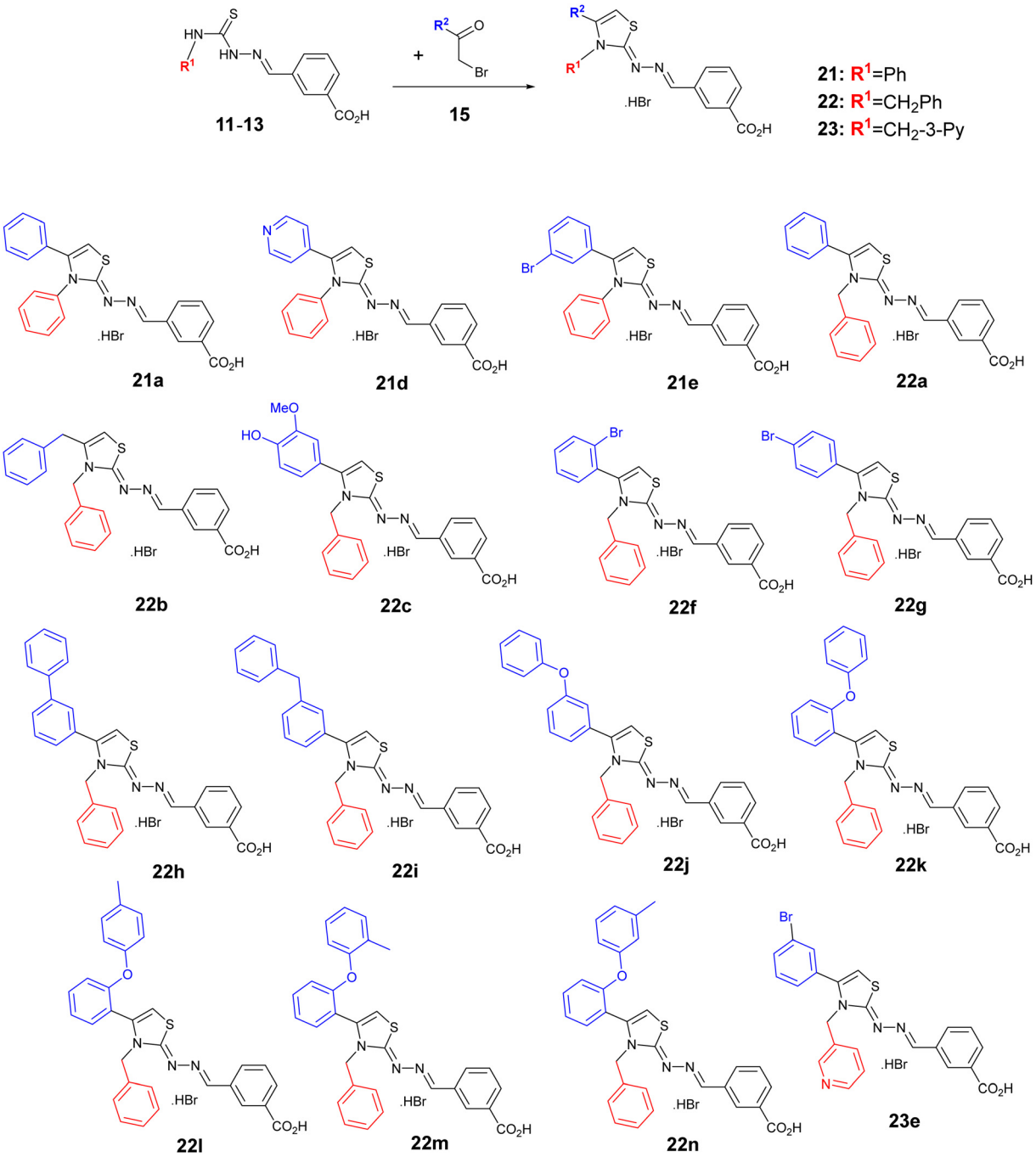

Scheme 5 Synthesis of the target molecules **21**, **22** and **23**.

Biological studies

To evaluate the biological activity of these molecules and to distinguish Mcl-1 inhibitors from Bcl-x_L inhibitors or dual inhibitors, we used an ovarian cancer cell line (IGROV1-R10) that depends on both Bcl-x_L and Mcl-1 for its survival, as previously described. Indeed, their concomitant inhibition leads to massive apoptosis, whereas inhibition of either Mcl-1 or Bcl-x_L alone does not.[9] Bcl-x_L or Mcl-1 were inhibited in IGROV1-R10 cells using specific siRNA (siBcl-x_L and siMcl-1) or pharmacological inhibitors (ABT-737[47] and S63845[48] respectively) and these cells were then exposed to the molecules of interest. The combination leading to cell death is thus indicative of the activity of the evaluated molecules.

No apoptosis was observed after exposure of these cells to siBcl-x_L or ABT-737 or to siMcl-1 or S63845 alone, while the combination of siBcl-x_L with siMcl-1 or ABT-737 with S63845 induced massive apoptotic cell death (Fig. 2A). Indeed, as previously described, these combinations lead to massive cell detachment and shrinkage, highly indicative of cell death. Our previous studies showed that under these conditions, caspase 3

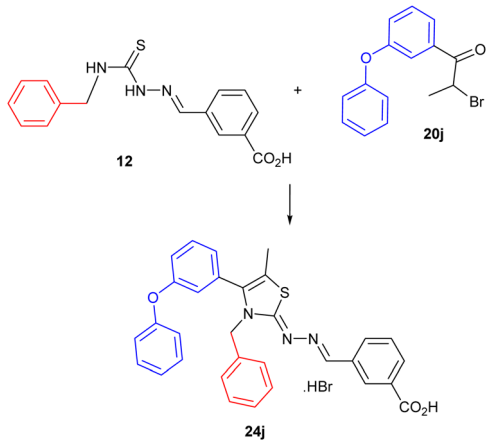

Scheme 6 Synthesis of the target molecule **24j**.

was activated and PARP cleavage was observed, showing the apoptotic nature of cell death.[11,44]

Based on morphological observations, we clearly excluded the possibility that compounds **21a**, **21d**, **21e** could be Bcl-x_L or Mcl-1 inhibitors since no combination led to cell death at 25 μM. However, the combination of compound **22a** with siBcl-x_L led to cell death, as demonstrated by cell detachment and shrinkage, while no such effects were observed in combination with siMcl-1 (Fig. 2B). These observations were confirmed by real-time caspase 3/7 activation assay since only compound **22a** showed an activation of caspase 3/7 after 24 h of treatment in association with siBcl-x_L and not with siMcl-1 (Fig. 2C). Together, these results show that compound **22a** is a potential Mcl-1 inhibitor.

The effects of compound **22a** on cell death in the IGROV1-R10 model were confirmed using pharmacological inhibitors (ABT-737 and S63845). The identification of optimal concentrations of both molecules to induce massive cell death in IGROV1-R10 was determined previously. Association of 5 μM of ABT-737 and 1 μM of S63845 was quite effective for inducing apoptosis, whereas neither of these molecules was able to induce cell death when used as a single agent at the indicated concentrations.[44]

Firstly, we observed that compound **22a** at 10 μM or 25 μM did not exert any effect (Fig. 3A and B, left panels). In contrast, combination of compound **22a** (at 10 μM or 25 μM) and ABT-737 (at 5 μM) induced cell detachment and shrinkage, condensation or fragmentation of nuclei, and increased the percentage of sub-G1 events, as shown in the DNA content histogram (Fig. 3A, middle panel), as well as the PARP and caspase 3 cleavage (Fig. 3B, left panel). As expected, compound **22a** was more effective at 25 μM than at 10 μM, as suggested by the percentage of sub-G1 events (40.9% for 25 μM *vs.* 30.6% for 10 μM) (Fig. 3A). Interestingly, the combination of compound **22a** and S63845 displayed no cytotoxic activity (Fig. 3A and B, right panels). Together, these results led us to conclude that compound **22a** can induce apoptosis in combination with the inhibition of Bcl-x_L in our model and to suggest that it is therefore a potential Mcl-1 inhibitor.

To improve the biological activity of compound **22a**, a second series of molecules was synthesized based on modulations of the aryl group in position 4 of the thiazole unit, and their activity was evaluated using impedancemetry, which allows medium- to high-throughput screening. This method allows growth curves to be established based on the cell index. Based on these tests, we exclude compounds **22b**, **22c**, **22f**, **22g**, **22h**, **22i**, **22j**, **22k**, **23e**, and **24j** as Bcl-x_L or Mcl-1 potential inhibitors since their combination with ABT-737 or S63845 did not result in a decrease in the cell index (Fig. 4). However, the combination of compound **22k** with ABT-737 led to a drastic decrease in the cell index compared to control conditions with compound **22k** or ABT-737 alone. Furthermore, such an effect was not observed in combination with S63845 (Fig. 4). Taken together, these results suggest that compound **22k** could be a potential Mcl-1 inhibitor (Table 1).

To further confirm the effect of compound **22k** on cell death, alone or in combination with pharmacological inhibitors of Bcl-x_L and Mcl-1, the effects on cell morphology, DNA fragmentation, percentage of sub-G1 events, and PARP and caspase 3 cleavage were assessed (Fig. 5A and B). While exposure to this compound as a single agent did not have any impact on these parameters, a massive apoptosis was observed in the presence of both compound **22k** and ABT-737, as demonstrated by the increase of cell detachment and sub-G1 events, nuclei fragmentation and PARP and caspase 3 cleavage (Fig. 5A and B). In contrast, the combination of compound **22k** and S63845 did not exert such cytotoxic effects on IGROV1-R10 cells, suggesting that this compound does not target Bcl-x_L and could thus be identified as a potential Mcl-1 inhibitor (Table 1).

Modification of compound **22k** led to the synthesis of new molecules (compounds **22l**, **22m**, **22n**) featuring a methyl at the end of the 2-diphenyl ether chain. Their biological activities, alone or in combination with pharmacological inhibitors of Bcl-x_L and Mcl-1 were then evaluated. As previously observed with compound **22k**, exposure to the compounds alone had no effect on apoptosis induction (Fig. 6, left panel). However, the effect was different between the molecules when they were combined with ABT-737 or S63845. For compound **22l**, we observed induction of massive apoptosis at 10 μM and 25 μM in combination with ABT-737, as demonstrated by the increase in cell detachment and sub-G1 events, nuclei fragmentation (Fig. 6A, middle panel) and PARP and caspase 3 cleavages at 25 μM notably (Fig. 6B, left panel). For compound **22m**, this effect was only observed at 25 μM (Fig. 6A, middle panel; Fig. 6B, left panel). Limited cleavage of PARP and caspase 3 was also observed at 25 μM of the compound in combination with S63845 (Fig. 6B, right panel). For compound **22n**, an apoptotic effect was observed at 25 μM in combination with ABT-737 (Fig. 6A, middle panel) but also with S63845 (Fig. 6A, right panel; Fig. 6B, right panel), which was not the case for compounds **22l** and **22m** at any concentration. Thus, compounds **22l** and **22m** could be potential inhibitors of Mcl-1, and compound **22n** a potential dual-action inhibitor of Mcl-1 and Bcl-x_L (Table 1).

Table 1 Summary of biological activity and predicted binding profiles of the selected compounds

Structure	Compound ID	Active at 10 μM	Active at 25 μM	Putative target	Notes
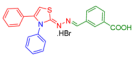	**21a**	No	N.A	Inactive	No significant activity observed
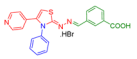	**21d**	No	N.A	Inactive	No significant activity observed
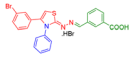	**21e**	No	N.A	Inactive	No significant activity observed
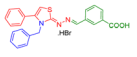	**22a**	Yes	Yes	Mcl-1	Activity observed only with Bcl-x_L inhibition
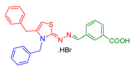	**22b**	No	N.A	Inactive	No significant activity observed
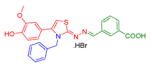	**22c**	No	N.A	Inactive	No significant activity observed
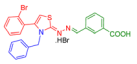	**22f**	No	N.A	Inactive	No significant activity observed
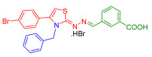	**22g**	No	N.A	Inactive	No significant activity observed
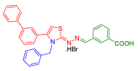	**22h**	No	N.A	Inactive	No significant activity observed
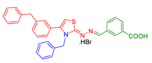	**22i**	No	N.A	Inactive	No significant activity observed
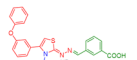	**22j**	No	N.A	Inactive	No significant activity observed
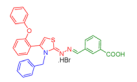	**22k**	Yes	Yes	Mcl-1	Activity observed only with Bcl-x_L inhibition
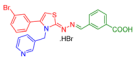	**23e**	No	N.A	Inactive	No significant activity observed
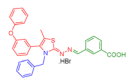	**24j**	No	N.A	Inactive	No significant activity observed
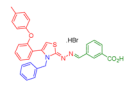	**22l**	Yes	Yes	Mcl-1	Activity observed only with Bcl-x_L inhibition
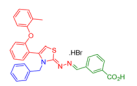	**22m**	No	Yes	Mcl-1	Activity observed only with Bcl-x_L inhibition
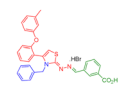	**22n**	No	Yes	Mcl-1 and Bcl-x_L	Activity observed with both Bcl-x_L and Mcl-1 inhibition

Molecular modelling studies

The binding mode of our previous lead compounds (see compounds numbers **27** and **35** in our first publication)[44] suggests that an isosteric replacement of the triphenol with a benzoic acid should be possible. Instead of forming multiple hydrogen bonds with D256 and R263, such a group could indeed form a unique and simple ionic interaction with R263. Since an ionic interaction is only dependent on the distance between charged groups, with fewer geometric constraints than for hydrogen bonds, such replacement could be more versatile for medicinal chemistry optimization. The corresponding **22a** confirmed this hypothesis, as judged by the biological testing we report above. The double benzyl-substituted thiazole (**22b**) could even fit better the geometry of the binding site, but, disappointingly, this molecule was inactive. Docking experiments were performed to understand these results. Surprisingly, they showed that **22a** reorients itself within the binding site, as compared with the previous derivative (**27**).[44] In order to form the expected salt bridge, the benzylic substituent of the thiazole is extracted from the deep hydrophobic cavity made up of L246, M250, V274, L290 and I297. It is now in a more exposed cavity lined with M231 and forms π-stacking with F228. This time, it is the phenyl group that orients towards the deep cavity, stacked with F270. As a

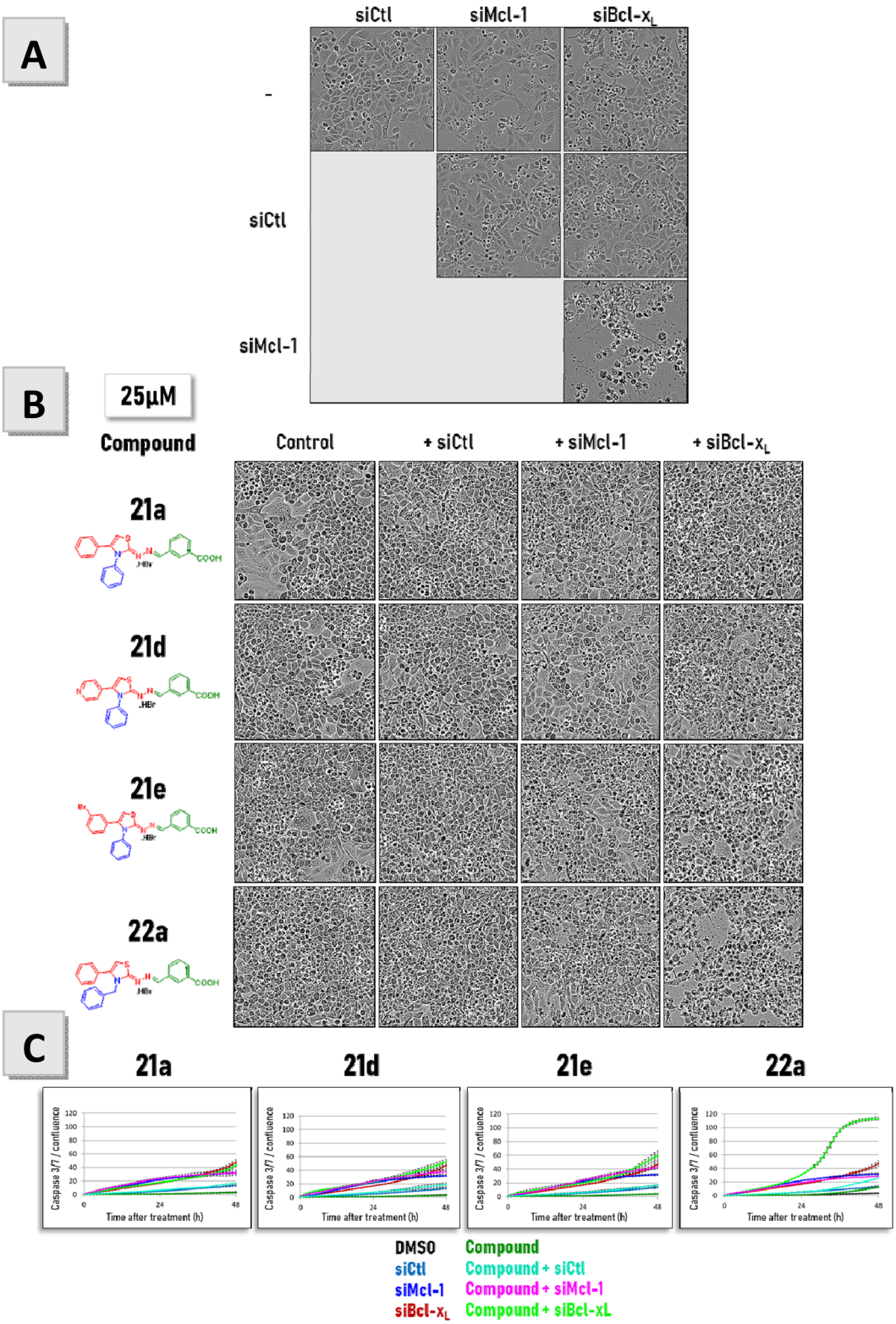

Fig. 2 Evaluation of the biological activity of compounds **21a**, **21d**, **21e** and **22a** on the IGROV1-R10 ovarian cancer cell line. (A) Morphology changes of ovarian cancer cells following 24 h exposure to 20 nM siRNA (siCtl, siMcl-1, siBcl-x_L) alone or in pairwise combination. (B) and (C) Ovarian cancer cells were treated with the indicated compounds at 10 μM for 48 h following exposure to 20 nM siRNA (siCtl, siMcl-1 or siBcl-x_L) for 24 h and (B) morphology changes and (C) real-time imaging of caspase 3/7 activation were assessed.

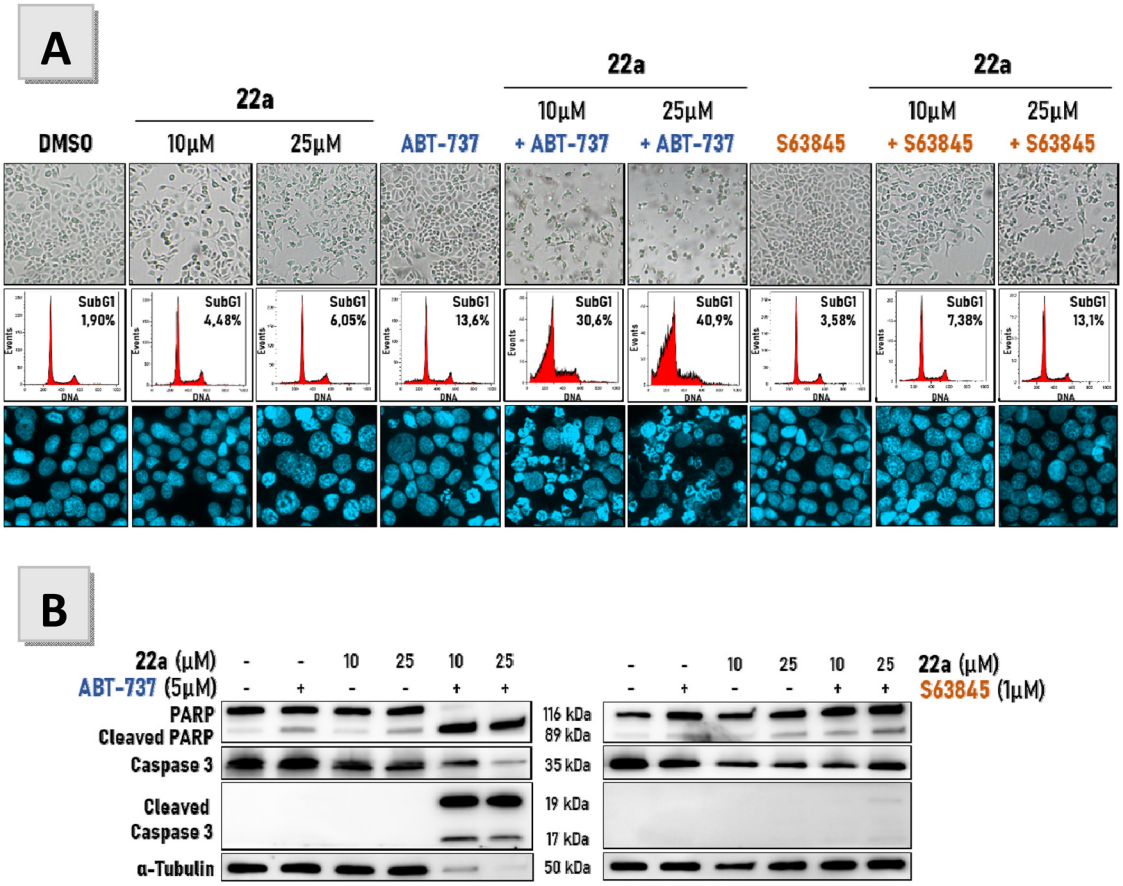

Fig. 3 Effect of compound **22a** in combination with Bcl-x_L or Mcl-1 inhibitors on apoptosis in the IGROV1-R10 ovarian cancer cell line. Cells were exposed to 10 or 25 μM of compound **22a** for 48 h alone or in combination with 5 μM of ABT-737 (Bcl-x_L inhibitor) or 1 μM of S63845 (Mcl-1 inhibitor). (A) Effects on the cellular morphology, DNA content, nuclear morphology and (B) on PARP and caspase 3 cleavages were assessed.

consequence, the double benzyl-substituted thiazole **22b** did not fill the cavities as expected (Fig. 7). One of its benzyl groups forms π-stacking with F270, while the second loses this type of interaction with F228. Moreover, the non-productive extra methylene of the second benzyl group adds an entropic penalty.

We then tried other substitutions of the thiazole. Contrary to our expectations, the benzoic acid is less tolerant than the phenol, since neither 4-methyl-pyridine (**21d**, as compared to the previous compound **25**), nor the double-phenyl (**21a**, as compared to the previous molecule **31**) is active. So, in the present case, forming a salt bridge is not simpler than forming three hydrogen bonds. This is probably due to the conjugation of the system thiazole-diaza-benzoic acid, which imposes a planar geometry of the ensemble, with no or less possible conformational adaptation.

Several small modifications around **21a** were not more promising, such as rendering its phenyl group more polar (**21d**) or, on the contrary, more hydrophobic (**21e**). The docking of **21a** showed that the molecule indeed reorients itself once again to preserve the salt bridge (Fig. 8). The RMSD between **22a** and **21a** is 3.7 Å, which implies different positions for the phenyl groups.

The docking of **22a** suggests that the *meta* position of the compound points in the direction of the deep hydrophobic cavity. Therefore, we tried different substitutions here to fill the pocket. However, introducing phenyl, benzyl or phenoxy groups proved to be unsuccessful (**22h**, **22i** and **22j**, respectively). We checked whether it was due to bad positioning of the substituent by introducing bromine in the *ortho* or *para* position (**22f** and **22g**, respectively), but these molecules were also inactive. Very surprisingly, an *ortho*-phenoxy group proved to be well tolerated (**22k**).

Docking of **22k** showed that its binding mode is more similar to that of **21a**, but its benzyl group is able to form π-stacking with F228. The *meta*-substituted analogue (**22j**) was inactive, probably because its phenoxy group is partly solvent-exposed, whereas that of **22k** is buried in the hydrophobic cavity and forms π-stacking with F270 (Fig. 9). Therefore, we tried a more polar analogue of **22j** (*para*-hydroxy and *meta*-methoxy instead of phenoxy). Unfortunately, the corresponding **22c** turned out to be inactive. On the contrary, the cavity where the phenoxy group binds is very hydrophobic, lined by F270, L267, V249 and M250. Moreover, it is large enough to accommodate a methyl substituent in every position (**22l**, **22m**, **22n**) (Fig. 10).

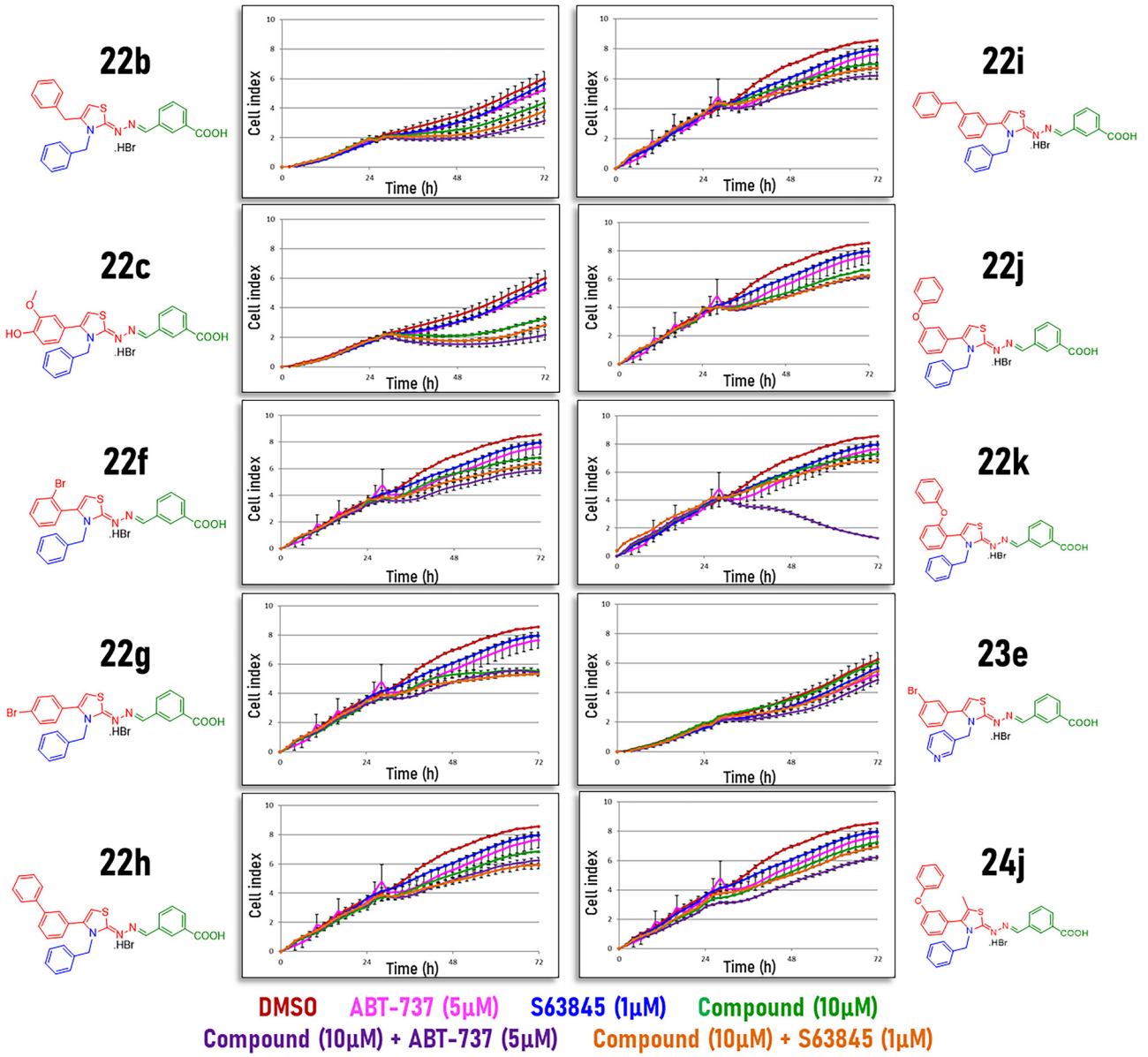

Fig. 4 Biological activity of compounds **22b**, **22c**, **22f**, **22g**, **22h**, **22i**, **22j**, **22k**, **23e** and **24j** in the IGROV1-R10 ovarian cancer cell line. Cells were exposed to the compounds at 10 μM alone or in combination with 5 μM of ABT-737 or 1 μM of S63845 24 h after the cells were seeded. Real-time cellular activity was assessed using impedancemetry. Impedance measurements from the first 48 hours of treatment are presented here.

Given that docking of **22a** showed that its benzyl group is partly exposed to the solvent, we tried to increase its hydrosolubility with a pyridine replacement. However, the corresponding **23e** was inactive.

Eventually, we tried to compensate for the lack of affinity of **22j** by adding extra contacts with the binding pocket, particularly by filling a small cavity formed by V249 and V253. Unfortunately, the resulting **24j** was still inactive.

Studies with our previous lead compound **35** have shown that the hydrophobicity of the thiazole substituents should favor Bcl-x_L, a close homologue of Mcl-1. Indeed, the position of **22k** in Bcl-x_L is reminiscent of the binding mode of this lead molecule **35**. However, an important aspect of this binding is the hydrogen bond network that the trisphenol engages with features charged side-chains, particularly D133 and E129. Here, the benzoic acid is a bad bioisoster, because it is not able to form said hydrogen bonds, and, worse, it is repelled by an electrostatic clash.

Experimental

– Chemical syntheses

General procedure 1 for the synthesis of imino-thiosemicarbazides 11–13

Representative procedure: synthesis of (*E*)-3-((2-(phenylcarbamothioyl)hydrazono)methyl)benzoic acid 11. An ethanolic

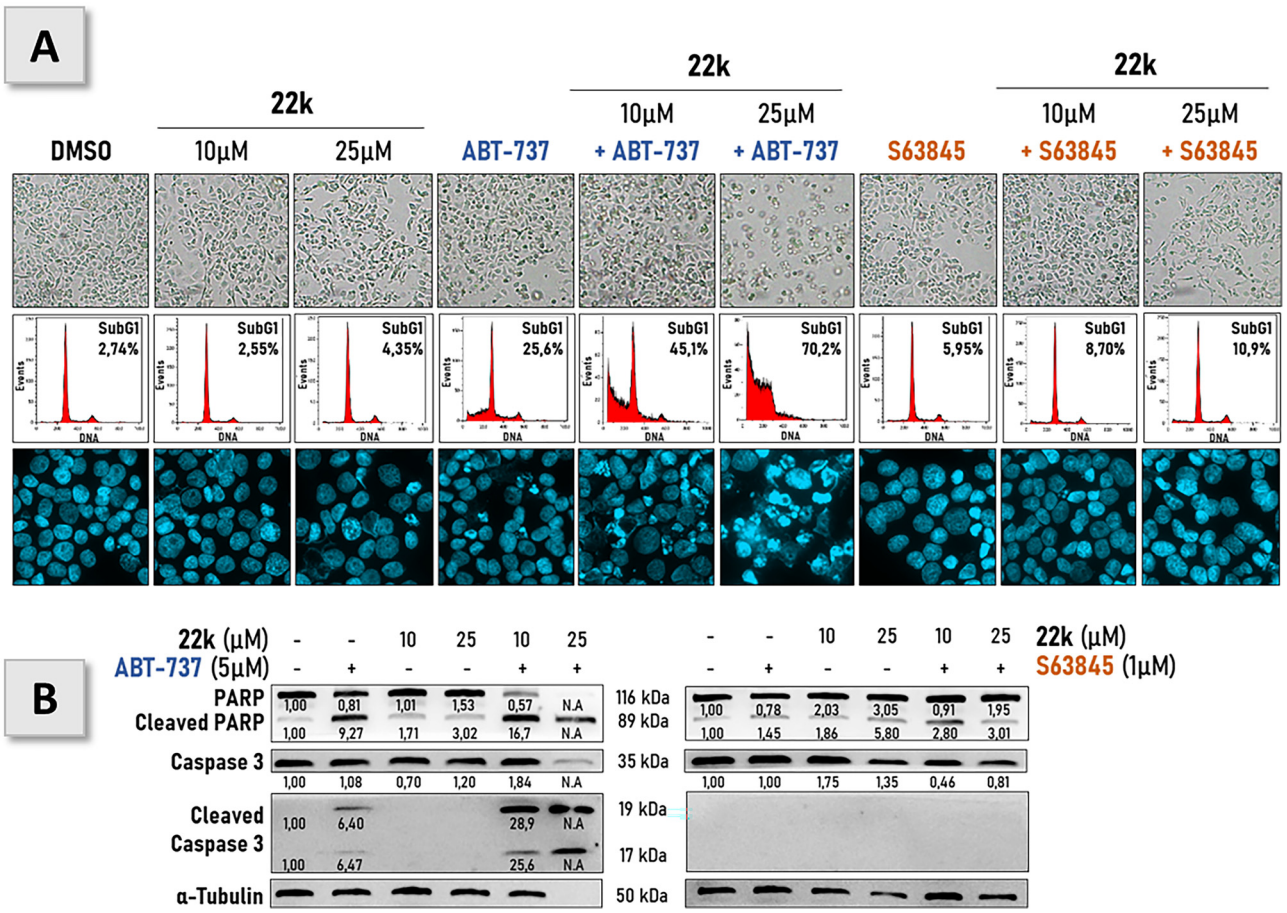

Fig. 5 Effect of compound **22k** in combination with Bcl-x_L or Mcl-1 inhibitors on apoptosis in the IGROV1-R10 ovarian cancer cell line. Cells were exposed to 10 or 25 μM of compound **22k** for 48 h alone or in combination with 5 μM of ABT-737 or 1 μM of S63845. (A) Effects on the cellular morphology, DNA content, nuclear morphology and (B) on PARP and caspase 3 cleavages (quantified relative to α-tubulin loading control) were assessed.

(20 mL) solution of thiourea **7** (2 g, 11.96 mmol) was added to a solution of 4-formylbenzoic acid **10** (2.7 g, 17.9 mmol) in ethanol (35 mL) and the reaction mixture was heated to reflux for 6 h. The product formed was filtered, washed with methanol and dried under vacuum to obtain (*E*)-3-((2-(phenylcarbamothioyl)hydrazono)methyl)benzoic acid **11** as a yellow solid, yield 3.1 g (86%). mp > 260 °C. ^{1}H NMR (500 MHz, DMSO-d_6) δ 13.16 (bs, 1H), 11.88 (s, 1H), 10.23 (s, 1H), 8.32–8.20 (m, 3H), 7.97 (dt, $^3J_{H-H}$ = 7.7 Hz, $^4J_{H-H}$ = 1.5 Hz, 1H), 7.60–7.52 (m, 3H), 7.43–7.32 (m, 2H), 7.27–7.17 (m, 1H). ^{13}C NMR (126 MHz, DMSO-d_6) δ 176.3, 167.1, 142.2, 139.1, 134.6, 131.4, 131.3, 130.6, 129.0, 128.7, 128.1, 126.2, 125.5. HRMS (ESI): calcd for [M + Na]$^+$ ($C_{15}H_{13}N_3O_2NaS$) = 322.0621; found: 322.0619 (0 ppm).

(*E*)-3-((2-(Benzylcarbamothioyl)hydrazono)methyl)benzoic acid 12. White solid, yield 2.9 g (85%) from 2 g (11.0 mmol) of **8**. mp = 235 °C. ^{1}H NMR (300 MHz, DMSO-d_6) δ 11.65 (s, 1H), 9.17 (t, $^3J_{H-H}$ = 6.2 Hz, 1H), 8.23 (t, $^4J_{H-H}$ = 1.7 Hz, 1H), 8.18 (s, 1H), 8.14 (dt, $^3J_{H-H}$ = 7.8 Hz, $^4J_{H-H}$ = 1.5 Hz, 1H), 7.95 (dt, $^3J_{H-H}$ = 7.8 Hz, $^4J_{H-H}$ = 1.5 Hz, 1H), 7.54 (t, $^3J_{H-H}$ = 7.8 Hz, 1H), 7.42–7.14 (m, 5H), 4.87 (d, $^3J_{H-H}$ = 6.2 Hz, 2H). ^{13}C NMR (75 MHz, DMSO-d_6) δ 177.7, 167.1, 141.7, 139.5, 134.7, 131.5, 131.1, 130.5, 129.0, 128.4, 128.2, 127.2, 126.8, 46.7. HRMS (ESI): calcd for [M + Na]$^+$ ($C_{16}H_{15}N_3O_2NaS$) = 336.0777; found: 336.0778 (0 ppm).

(*E*)-3-((2-((Pyridin-3-ylmethyl)carbamothioyl)hydrazono)methyl)-benzoic acid 13. Yellow solid, yield 664 mg (77%) from 500 mg (2.7 mmol) of **9** and 616 g (4.1 mmol) of **10**. mp = 215 °C. ^{1}H NMR (300 MHz, DMSO-d_6) δ 13.17 (s, 1H), 11.72 (s, 1H), 9.24 (t, $^3J_{H-H}$ = 6.2 Hz, 1H), 8.58 (d, $^4J_{H-H}$ = 2.2 Hz, 1H), 8.45 (dd, $^3J_{H-H}$ = 4.8 Hz, $^4J_{H-H}$ = 1.7 Hz, 1H), 8.24 (s, 1H), 8.17 (s, 1H), 8.13 (dt, $^3J_{H-H}$ = 7.8 Hz, $^4J_{H-H}$ = 1.5 Hz, 1H), 7.96 (dt, $^3J_{H-H}$ = 7.7 Hz, $^4J_{H-H}$ = 1.4 Hz, 1H), 7.77 (dd, $^3J_{H-H}$ = 7.9 Hz, $^4J_{H-H}$ = 2.0 Hz, 1H), 7.55 (t, $^3J_{H-H}$ = 7.7 Hz, 1H), 7.36 (dd, $^3J_{H-H}$ = 7.7 Hz, $^3J_{H-H}$ = 4.8 Hz, 1H), 4.87 (d, $^3J_{H-H}$ = 6.2 Hz, 2H). ^{13}C NMR (75 MHz, DMSO-d_6) δ 177.8, 167.0, 148.8, 148.0, 142.0, 135.1, 135.0, 134.6, 131.5, 131.1, 130.5, 129.0, 128.3, 123.4, 44.4. HRMS (ESI): calcd for [M + Na]$^+$ ($C_{15}H_{14}N_4O_2NaS$) = 337.0735; found: 337.0736 (1 ppm).

General procedure 2 for the synthesis of bromoketones 15h–n

To the aryl-ketones **14h–n** (0.90 mmol) in ethyl acetate (2 mL) was added $CuBr_2$ (200 mg, 0.90 mmol) under magnetic stirring at 70 °C and the reaction was monitored by TLC. The reaction mixture was filtered and the filtrate was evaporated and

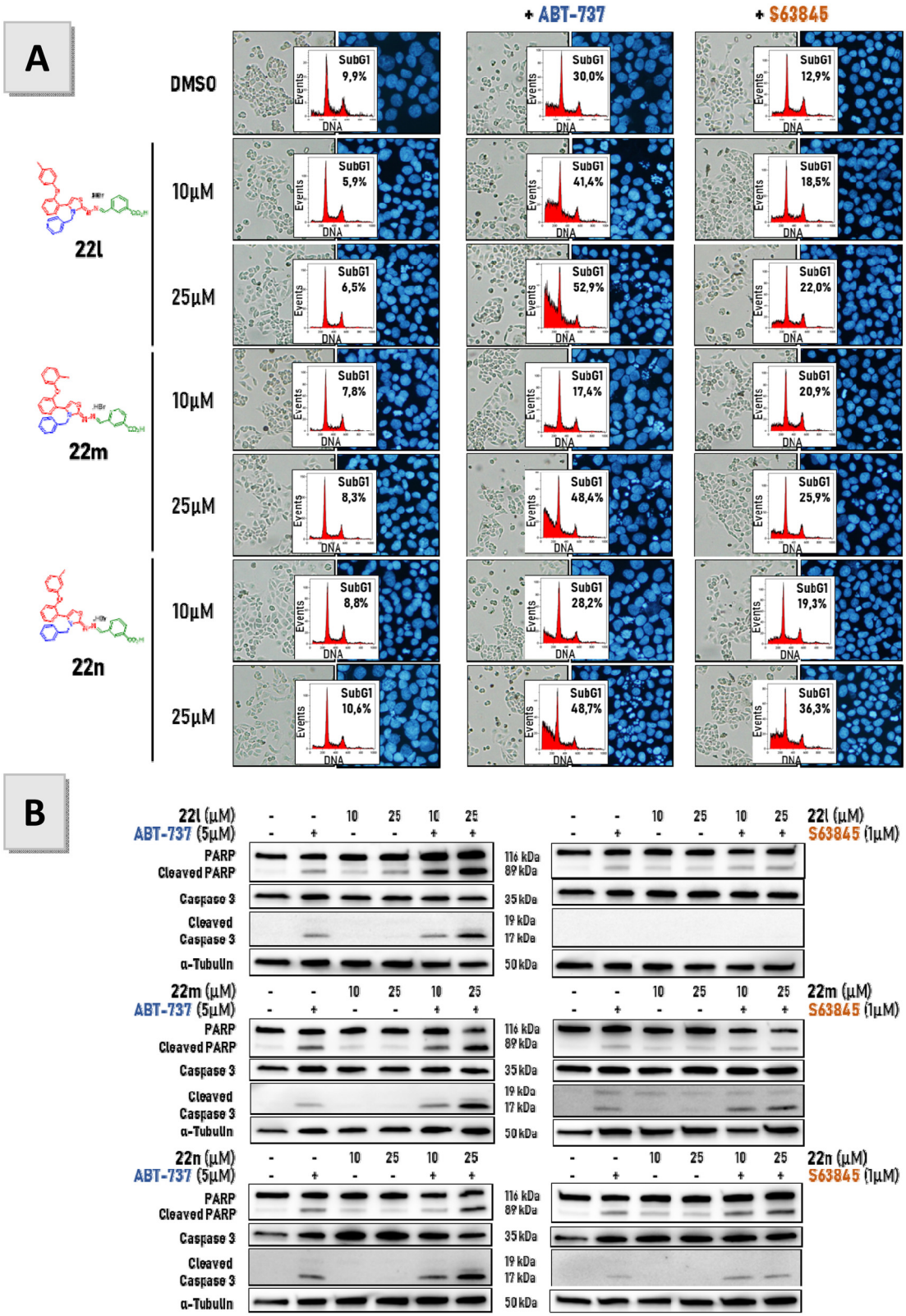

Fig. 6 Effect of compounds **22l**, **22m** and **22n** in combination with Bcl-x_L or Mcl-1 inhibitors on apoptosis in the IGROV1-R10 ovarian cancer cell line. Cells were exposed to 10 or 25 μM of compound **22l**, **22m** or **22n** for 24 h alone or in combination with 5 μM of ABT-737 or 1 μM of S63845. (A) Effects on the cellular morphology, DNA content, nuclear morphology and (B) on PARP and caspase 3 cleavage were assessed.

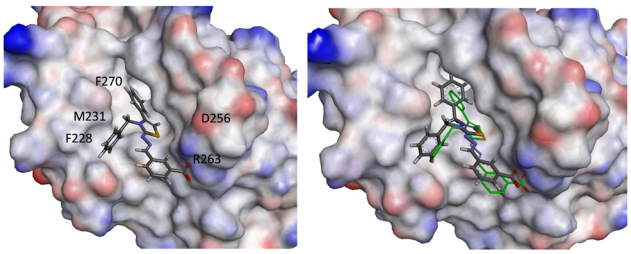

Fig. 7 Binding mode in Mcl-1 of **22a** (left) as suggested by docking experiments. On the right, **22b** is superimposed on **22a** (thin bonds with carbon atoms in green). The Connolly surface of the protein is colored according to its electrostatic potential: blue for positive charges and red for negative charges.

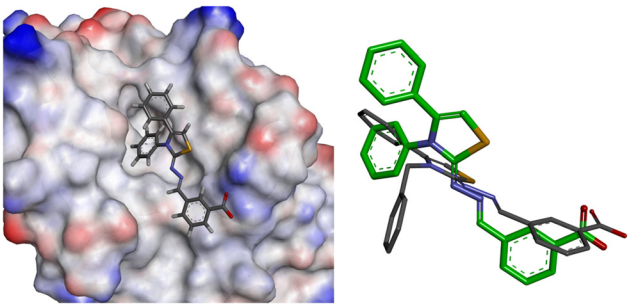

Fig. 8 Binding mode in Mcl-1 of **21a** (left) as suggested by docking experiments. Superimposition of **21a** and **22a** as docked in the binding site (right). A RMSD of 3.7 Å can be calculated between the common part of the scaffold.

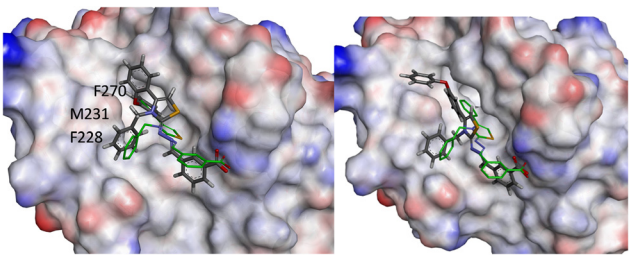

Fig. 9 Binding mode in Mcl-1 of **22k** (left) and **22j** (right) as suggested by docking experiments. Both compounds are superposed on **22a** (thin bonds with carbon atoms in green).

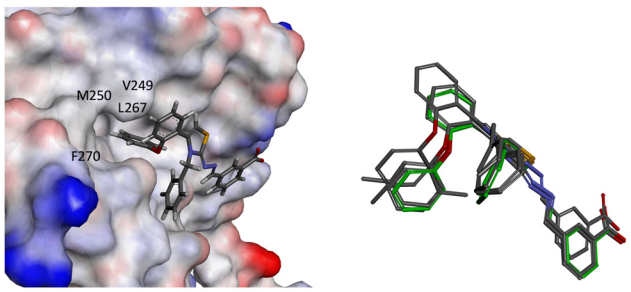

Fig. 10 Binding mode of **22k** in Mcl-1 (left). On the right, its methylated derivatives **22l**, **22m**, **22n** are superimposed within the binding site, as suggested by docking experiments (**22k** bonds have carbon atoms in green).

purified by chromatography on silica gel to obtain bromoketones **15h–n**.

1-([1,1′-Biphenyl]-3-yl)-2-bromoethan-1-one 15h. Colorless oil, yield 203 mg (82%) starting from 3′-phenyl-acetophenone **14h** (177 mg, 0.90 mmol). NMR data in accordance to E. Moine *et al. Eur. J. Med. Chem.*, 2015, **105**, 80–105. ^{1}H NMR (300 MHz, $CDCl_3$) δ 8.21 (td, $^{4}J_{H-H}$ = 1.8 Hz, $^{4}J_{H-H}$ = 0.5 Hz 1H), 7.96 (ddd, $^{3}J_{H-H}$ = 7.8 Hz, $^{4}J_{H-H}$ = 1.8 Hz, $^{4}J_{H-H}$ = 1.1 Hz, 1H), 7.84 (ddd, $^{3}J_{H-H}$ = 7.8 Hz, $^{4}J_{H-H}$ = 1.8 Hz, $^{4}J_{H-H}$ = 1.1 Hz, 1H), 7.65–7.39 (m, 6H), 4.52 (s, 2H). ^{13}C NMR (75 MHz, $CDCl_3$) δ 191.4, 142.2, 140.0, 134.6, 132.7, 129.4, 129.1, 129.1, 128.1, 127.8, 127.8, 127.3, 127.3, 31.0.

1-(3-Benzylphenyl)-2-bromoethan-1-one 15i. Colorless oil, yield 229 mg (88%) starting from **14i** (189 mg, 0.90 mmol). ^{1}H NMR (300 MHz, $CDCl_3$) δ 7.92–7.76 (m, 2H), 7.48–7.35 (m, 2H), 7.37–7.25 (m, 2H), 7.25–7.15 (m, 3H), 4.43 (s, 2H), 4.05 (s, 2H). ^{13}C NMR (75 MHz, $CDCl_3$) δ 191.4, 142.1, 140.1, 134.6, 134.2, 129.3, 129.0, 128.9, 128.7, 126.9, 126.5, 41.7, 31.1.

2-Bromo-1-(3-phenoxyphenyl)ethan-1-one 15j. Colorless oil, yield 220 mg (84%) starting from **14j** (191 mg, 0.90 mmol). ^{1}H NMR (300 MHz, $CDCl_3$) δ 7.70 (ddd, $^{3}J_{H-H}$ = 7.7 Hz, $^{4}J_{H-H}$ = 1.7 Hz, $^{4}J_{H-H}$ = 1.0 Hz, 1H), 7.60 (dd, $^{4}J_{H-H}$ = 2.5 Hz, $^{4}J_{H-H}$ = 1.6 Hz, 1H), 7.45 (t, $^{3}J_{H-H}$ = 8.0 Hz, 1H), 7.42–7.32 (m, 2H), 7.28–7.22 (m, 1H), 7.20–7.11 (m, 1H), 7.08–6.98 (m, 2H), 4.41 (s, 2H). ^{13}C NMR (75 MHz, $CDCl_3$) δ 190.8, 158.2, 156.4, 135.8, 130.4, 130.2, 124.2, 124.2, 123.6, 119.4, 118.6, 31.0.

2-Bromo-1-(2-phenoxyphenyl)ethan-1-one 15k. Colorless oil, yield 197 mg (75%) starting from **14k** (191 mg, 0.90 mmol). ^{1}H NMR (300 MHz, $CDCl_3$) δ 7.92 (dd, $^{3}J_{H-H}$ = 7.9 Hz, $^{4}J_{H-H}$ = 1.8 Hz, 1H), 7.53–7.35 (m, 3H), 7.25–7.13 (m, 2H), 7.13–7.04 (m, 2H), 6.86 (dd, $^{3}J_{H-H}$ = 8.4 Hz, $^{4}J_{H-H}$ = 1.1 Hz, 1H), 4.65 (s, 2H). ^{13}C NMR (75 MHz, $CDCl_3$) δ 192.0, 157.0, 155.4, 134.7, 131.8, 130.4, 126.7, 124.9, 123.4, 119.9, 118.1, 37.3.

2-Bromo-1-(2-(*p*-tolyloxy)phenyl)ethan-1-one 15l. Yellow oil, yield 220 mg (80%) starting from **14l** (205 mg, 0.90 mmol). ^{1}H NMR (300 MHz, $CDCl_3$) δ 7.91 (dd, $^{3}J_{H-H}$ = 7.9 Hz, $^{4}J_{H-H}$ = 1.8 Hz, 1H), 7.43 (ddd, $^{3}J_{H-H}$ = 8.4 Hz, $^{3}J_{H-H}$ = 7.3 Hz, $^{4}J_{H-H}$ = 1.8 Hz, 1H), 7.23–7.18 (m, 2H), 7.14 (ddd, $^{3}J_{H-H}$ = 7.9 Hz, $^{3}J_{H-H}$ = 7.3 Hz, $^{4}J_{H-H}$ = 1.0 Hz, 1H), 7.02–6.96 (m, 2H), 6.83 (dd, $^{3}J_{H-H}$ = 8.4 Hz, $^{4}J_{H-H}$ = 1.0 Hz, 2H), 4.66 (s, 2H), 2.37 (s, 3H). ^{13}C NMR (75 MHz, $CDCl_3$) δ 192.2, 157.5, 153.0, 134.7, 134.6, 131.7, 130.8, 126.4, 123.1, 120.0, 117.6, 37.4, 20.9.

2-Bromo-1-(2-(*o*-tolyloxy)phenyl)ethan-1-one 15m. Yellow oil, yield 217 mg (79%) starting from **14m** (205 mg, 0.90 mmol). ^{1}H NMR (300 MHz, $CDCl_3$) δ 7.93 (ddd, $^{3}J_{H-H}$ = 7.8 Hz, $^{4}J_{H-H}$ = 1.8 Hz, $^{5}J_{H-H}$ = 0.4 Hz, 1H), 7.40 (ddd, $^{3}J_{H-H}$ = 8.4 Hz, $^{3}J_{H-H}$ = 7.3 Hz, $^{4}J_{H-H}$ = 1.8 Hz, 1H), 7.34–7.29 (m, 1H), 7.25–7.20 (m, 1H), 7.18 (dd, $^{3}J_{H-H}$ = 7.3 Hz, $^{4}J_{H-H}$ = 1.5 Hz, 1H), 7.12 (ddd, $^{3}J_{H-H}$ = 7.8 Hz, $^{3}J_{H-H}$ = 7.3 Hz, $^{4}J_{H-H}$ = 1.1 Hz, 1H), 6.98 (dd, $^{3}J_{H-H}$ = 7.8 Hz, $^{4}J_{H-H}$ = 1.5 Hz, 1H), 4.71 (s, 2H), 2.26 (s, 4H). ^{13}C NMR (75 MHz, $CDCl_3$) δ 192.1, 157.4, 152.9, 134.8, 132.0, 131.9, 130.5, 127.8, 125.7, 125.5, 122.7, 120.6, 116.2, 37.4, 16.4.

2-Bromo-1-(2-(*m*-tolyloxy)phenyl)ethan-1-one 15n. Yellow oil, yield 217 mg (79%) starting from **14n** (205 mg, 0.90 mmol). ^{1}H NMR (300 MHz, $CDCl_3$) δ 7.92 (ddd, $^{3}J_{H-H}$ = 7.8 Hz, $^{4}J_{H-H}$ = 1.8 Hz, $^{5}J_{H-H}$ = 0.4 Hz, 1H), 7.45 (ddd, $^{3}J_{H-H}$ = 8.3 Hz, $^{3}J_{H-H}$ = 7.3 Hz,

$^4J_{H-H}$ = 1.8 Hz, 1H), 7.34–7.23 (m, 1H), 7.16 (ddd, $^3J_{H-H}$ = 7.8 Hz, $^3J_{H-H}$ = 7.3 Hz, $^4J_{H-H}$ = 1.1 Hz, 1H), 7.05–7.00 (m, 1H), 6.93–6.84 (m, 3H), 4.65 (s, 2H), 2.37 (s, 3H). ^{13}C NMR (75 MHz, $CDCl_3$) δ 192.1, 157.1, 155.4, 140.7, 134.7, 131.7, 130.0, 126.6, 125.7, 123.3, 120.5, 118.1, 116.9, 37.4, 21.5.

Procedure for the synthesis of bromoketone 20j

Synthesis of 1-(3-phenoxyphenyl)propan-1-ol 18. To 3-phenoxybenzaldehyde **16** (813 mg, 4.1 mmol) in THF (25 mL) was added ethylmagnesium bromide solution **17** (1.5 equiv.) under nitrogen gas at 0 °C. The reaction was monitored by TLC, then saturated NH_4Cl (10 mL) was added, and the reaction mixture was extracted with ethyl acetate (3 × 20 mL). The organic layers were separated, washed with water (1 × 10 mL), dried over Na_2SO_4, and concentrated under vacuum. After purification by chromatography on silica gel, alcohol **18** (467 mg, 50%) was obtained as a colorless oil. ^{1}H NMR (300 MHz, $CDCl_3$) δ 7.39–7.27 (m, 3H), 7.17–7.05 (m, 2H), 7.04–6.97 (m, 3H), 6.91 (ddd, $^3J_{H-H}$ = 8.1 Hz, $^4J_{H-H}$ = 2.5 Hz, $^4J_{H-H}$ = 1.0 Hz, 1H), 4.58 (t, $^3J_{H-H}$ = 6.5 Hz, 1H), 1.83–1.70 (m, 3H), 0.92 (t, $^3J_{H-H}$ = 7.4 Hz, 3H). ^{13}C NMR (75 MHz, $CDCl_3$) δ 157.5, 157.3, 146.9, 129.9, 129.8, 123.4, 120.9, 119.0, 117.9, 116.6, 75.8, 32.0, 10.2.

Synthesis of 1-(3-phenoxyphenyl)propan-1-one 19. To the obtained alcohol **18** (1.24 mmol) in acetone (10 mL) was added dropwise under magnetic stirring at room temperature, a concentrated (5.4 M) solution of Jones reagent until the disappearance of the starting material (TLC analysis). After addition of isopropanol (5.0 equiv.), the reaction mixture was filtered and the filtrate was extracted with ethyl acetate (3 × 40 mL). The combined organic phases were dried over Na_2SO_4, filtered, and concentrated *in vacuo*. After purification by chromatography on silica gel, the ketone **19** was obtained as a colorless oil, yield 266 mg (95%). ^{1}H NMR (300 MHz, $CDCl_3$) δ 7.69 (ddd, $^3J_{H-H}$ = 7.7 Hz, $^4J_{H-H}$ = 1.6 Hz, $^4J_{H-H}$ = 1.1 Hz, 1H), 7.59 (dd, $^4J_{H-H}$ = 2.5 Hz, $^4J_{H-H}$ = 1.6 Hz, 1H), 7.46–7.32 (m, 3H), 7.22–7.10 (m, 2H), 7.05–6.97 (m, 2H), 2.96 (q, $^3J_{H-H}$ = 7.3 Hz, 2H), 1.21 (t, $^3J_{H-H}$ = 7.3 Hz, 3H). ^{13}C NMR (75 MHz, $CDCl_3$) δ 200.3, 157.9, 156.8, 138.9, 130.1, 130.1, 123.9, 123.3, 122.9, 119.2, 118.0, 32.1, 8.3.

Synthesis of 2-bromo-1-(3-phenoxyphenyl)propan-1-one 20j. To the aryl-ketone **19** (0.90 mmol) in ethyl acetate (2 mL) was added $CuBr_2$ (200 mg, 0.90 mmol) under magnetic stirring at 70 °C and the reaction was monitored by TLC. The reaction mixture was filtrated and the filtrate was evaporated and purified by chromatography on silica gel to obtain bromoketone **20j** as a colorless oil, yield 206 mg (75%). ^{1}H NMR (300 MHz, $CDCl_3$) δ 7.75 (ddd, $^3J_{H-H}$ = 7.7 Hz, $^4J_{H-H}$ = 1.7 Hz, $^4J_{H-H}$ = 1.0 Hz, 1H), 7.67–7.62 (m, 1H), 7.44 (t, $^3J_{H-H}$ = 8.0 Hz, 1H), 7.41–7.33 (m, 2H), 7.23 (ddd, $^3J_{H-H}$ = 8.2 Hz, $^4J_{H-H}$ = 2.5 Hz, $^4J_{H-H}$ = 1.0 Hz, 1H), 7.19–7.12 (m, 1H), 7.07–7.00 (m, 2H), 5.22 (q, $^3J_{H-H}$ = 6.6 Hz, 1H), 1.89 (d, $^3J_{H-H}$ = 6.6 Hz, 3H). ^{13}C NMR (75 MHz, $CDCl_3$) δ 192.8, 158.0, 156.5, 135.9, 130.2, 130.1, 124.1, 123.9, 123.6, 119.4, 118.7, 41.6, 20.2.

General procedure for the synthesis of target molecules 21, 22, 23 and 24

A mixture of the appropriate intermediate **11–13** (0.4 mmol) and bromoketone **15a–n** and **20j** (0.8 mmol) in ethanol (10 mL) was heated to reflux for 6 h. The mixture was concentrated and the solid obtained was washed using acetone several times to obtain the desired product.

3-((*E*)-(((*E*)-3,4-Diphenylthiazol-2(3*H*)-ylidene)hydrazono)-methyl)benzoic acid hydrobromide 21a. The product (169 mg, 88%) was obtained as a yellow solid. mp > 260 °C. ^{1}H NMR (500 MHz, DMSO-d_6) δ 8.32 (s, 1H), 8.28 (s, 1H), 7.96 (d, $^3J_{H-H}$ = 7.7 Hz, 1H), 7.92 (d, $^3J_{H-H}$ = 7.8 Hz, 1H), 7.57 (t, $^3J_{H-H}$ = 7.7 Hz, 1H), 7.46–7.34 (m, 5H), 7.32–7.14 (m, 5H), 6.91 (s, 1H). ^{13}C NMR (126 MHz, DMSO-d_6) δ 170.4, 167.0, 150.8, 140.6, 136.3, 134.9, 131.4, 130.7, 129.9, 129.4, 129.3, 129.0, 128.9, 128.8, 128.7, 128.3, 127.6, 103.9. HRMS (ESI): calcd for $[M + Na]^+$ ($C_{23}H_{17}N_3O_2NaS$) = 422.0933; found: 422.0932.

3-((*E*)-(((*E*)-3-Phenyl-4-(pyridin-4-yl)thiazol-2(3*H*)-ylidene)hydrazineylidene)methyl)benzoic acid hydrobromide 21d. The product (77 mg, 40%) was obtained as a yellow solid. mp = 240 °C (pyrolysis). ^{1}H NMR (500 MHz, DMSO-d_6) δ 8.79 (s, 1H), 8.78 (s, 1H), 8.32 (s, 1H), 8.30 (s, 1H), 7.94 (t, $^3J_{H-H}$ = 8.3 Hz, 2H), 7.69 (d, $^3J_{H-H}$ = 5.9 Hz, 2H), 7.59 (s, 1H), 7.56 (t, $^3J_{H-H}$ = 7.7 Hz, 1H), 7.51–7.35 (m, 5H). ^{13}C NMR (126 MHz, DMSO-d_6) δ 169.8, 167.0, 152.2, 145.2, 142.4, 136.7, 135.4, 135.2, 131.5, 131.4, 130.5, 129.5, 129.2, 128.8, 128.4, 127.6, 124.3, 112.9. HRMS (ESI): calcd for $[M + Na]^+$ ($C_{22}H_{16}N_4O_2NaS$) = 423.0886; found: 423.0884.

3-((*E*)-(((*E*)-4-(3-Bromophenyl)-3-phenylthiazol-2(3*H*)-ylidene)-hydrazineylidene)methyl)benzoic acid hydrobromide 21e. The product (145 mg, 65%) was obtained as a yellow solid. mp = 211 °C. ^{1}H NMR (500 MHz, DMSO-d_6) δ 8.30 (s, 1H), 8.27 (s, 1H), 7.95 (d, $^3J_{H-H}$ = 7.7 Hz, 1H), 7.92 (d, $^3J_{H-H}$ = 7.4 Hz, 1H), 7.56 (t, $^3J_{H-H}$ = 7.7 Hz, 1H), 7.52–7.31 (m, 7H), 7.26–7.10 (m, 2H), 6.98 (s, 1H). ^{13}C NMR (126 MHz, DMSO-d_6) δ 170.3, 167.0, 150.9, 138.7, 136.4, 135.0, 132.2, 131.6, 131.4, 131.2, 130.5, 130.4, 129.4, 129.2, 128.9, 128.8, 127.6, 127.6, 121.4, 104.6. HRMS (ESI): calcd for $[M + Na]^+$ ($C_{23}H_{16}N_3O_2{}^{79}BrNaS$) = 500.0038; found: 500.0036.

3-((*E*)-(((*E*)-3-Benzyl-4-phenylthiazol-2(3*H*)-ylidene)hydrazin-eylidene)methyl)benzoic acid hydrobromide 22a. The product (178 mg, 90%) was obtained as a yellow solid. mp > 260 °C. ^{1}H NMR (300 MHz, DMSO-d_6) δ 8.34 (s, 1H), 8.29 (s, 1H), 7.93 (dd, $^3J_{H-H}$ = 7.7, $^4J_{H-H}$ = 1.6 Hz, 2H), 7.55 (t, $^3J_{H-H}$ = 7.7 Hz, 1H), 7.50–7.14 (m, 9H), 6.98 (d, J = 6.7 Hz, 2H), 6.58 (s, 1H), 5.10 (s, 2H). ^{13}C NMR (75 MHz, DMSO-d_6) δ 170.2, 167.1, 149.9, 140.5, 136.6, 135.5, 131.4, 131.2, 130.2, 130.1, 129.5, 129.2, 129.0, 128.8, 128.6, 127.5, 127.3, 126.3, 101.9, 48.4. HRMS (ESI): calcd for $[M + Na]^+$ ($C_{24}H_{19}N_3O_2NaS$) = 414.1271; found: 414.1274.

3-((*E*)-(((*Z*)-3,4-Dibenzylthiazol-2(3*H*)-ylidene)hydrazono)-methyl)benzoic acid hydrobromide 22b. The product (103 mg, 51%) was obtained as a faded green solid. mp = 241 °C. ^{1}H NMR (300 MHz, methanol-d_4) δ 8.41–8.34 (m, 2H), 8.18–8.08 (m, 1H), 8.05–7.94 (m, 1H), 7.66–7.54 (m, 1H), 7.47–7.23 (m, 6H), 7.23–7.17 (m, 2H), 7.16–7.08 (m, 2H), 6.74 (s, 1H), 5.48 (s, 2H), 3.95 (s, 2H). ^{13}C NMR (75 MHz, methanol-d_4) δ 171.4, 168.7, 152.1, 144.1, 136.0, 134.6, 134.1, 133.5, 133.0, 132.9, 130.5, 130.4, 130.2, 130.0, 129.9, 129.6, 128.7, 126.7, 108.8, 51.0, 34.6. HRMS (ESI): calcd for $[M + Na]^+$ ($C_{25}H_{21}N_3O_2NaS$) = 450.1246; found: 450.1242.

3-((*E*)-(((*Z*)-3-Benzyl-4-(4-hydroxy-3-methoxyphenyl)thiazol-2(3*H*)-ylidene)hydrazono)methyl)benzoic acid hydrobromide 22c. The product (102 mg, 47%) was obtained as a yellow

solid. mp = 175 °C. ^{1}H NMR (300 MHz, methanol-d_4) δ 8.49–8.34 (m, 2H), 8.15 (dt, $^3J_{H-H}$ = 7.8, $^4J_{H-H}$ = 1.5 Hz, 1H), 8.02 (dt, $^3J_{H-H}$ = 7.8, $^4J_{H-H}$ = 1.5 Hz, 1H), 7.62 (t, $^3J_{H-H}$ = 7.8 Hz, 1H), 7.48–7.27 (m, 3H), 7.17–7.02 (m, 3H), 6.84 (s, 2H), 6.71 (s, 1H), 5.35 (s, 2H), 3.55 (s, 3H). ^{13}C NMR (75 MHz, methanol-d_4) δ 170.7, 168.8, 152.1, 150.3, 149.0, 145.3, 135.0, 134.6, 133.5, 133.1, 132.9, 132.9, 130.4, 129.9, 129.5, 127.0, 124.5, 120.1, 116.6, 114.0, 108.8, 56.2, 52.1. HRMS (ESI): calcd for $[M - H]^-$ ($C_{25}H_{20}N_3O_4S$) = 45.118; found: 45.118.

3-((*E*)-(((*Z*)-3-Benzyl-4-(2-bromophenyl)thiazol-2(3*H*)-ylidene)hydrazono)methyl)benzoic acid hydrobromide 22f. The product (181 mg, 79%) was obtained as a yellow solid. ^{1}H NMR (300 MHz, DMSO-d_6) δ 8.35 (s, 1H), 8.29 (t, $^4J_{H-H}$ = 1.7 Hz, 1H), 7.94 (d, $^4J_{H-H}$ = 1.7 Hz, 1H), 7.92 (d, $^4J_{H-H}$ = 1.7 Hz, 1H), 7.74 (dd, $^3J_{H-H}$ = 7.7, $^4J_{H-H}$ = 1.7 Hz, 1H), 7.55 (t, $^3J_{H-H}$ = 7.7 Hz, 1H), 7.39 (pd, $^3J_{H-H}$ = 7.4, $^4J_{H-H}$ = 1.7 Hz, 2H), 7.30–7.15 (m, 4H), 6.96–6.89 (m, 2H), 6.60 (s, 1H), 5.19 (d, $^2J_{H-H}$ = 16.2 Hz, 1H), 4.63 (d, $^2J_{H-H}$ = 16.2 Hz, 1H). ^{13}C NMR (75 MHz, DMSO-d_6) δ 169.6, 167.2, 150.0, 138.3, 136.2, 136.1, 135.6, 132.9, 132.1, 131.5, 131.3, 131.0, 130.6, 130.3, 129.3, 128.6, 128.0, 127.6, 126.8, 124.3, 103.3, 48.3. HRMS (ESI): calcd for $[M + Na]^+$ ($C_{24}H_{18}N_3O_2{}^{79}BrNaS$) = 514.0195; found: 514.0194.

3-((*E*)-(((*Z*)-3-Benzyl-4-(4-bromophenyl)thiazol-2(3*H*)-ylidene)hydrazono)methyl)benzoic acid hydrobromide 22g. The product (174 mg, 76%) was obtained as a yellow solid. mp = 250 °C. ^{1}H NMR (300 MHz, DMSO-d_6) δ 8.36 (s, 1H), 8.29 (t, $^4J_{H-H}$ = 1.7 Hz, 1H), 7.99–7.88 (m, 2H), 7.66–7.51 (m, 3H), 7.32–7.17 (m, 5H), 7.00–6.94 (m, 2H), 6.68 (s, 1H), 5.13 (s, 2H). ^{13}C NMR (75 MHz, DMSO-d_6) δ 170.1, 167.1, 150.2, 139.5, 136.2, 135.2, 131.8, 131.4, 131.4, 131.1, 130.4, 129.3, 129.2, 128.7, 127.6, 127.5, 126.3, 123.1, 103.4, 48.7. HRMS (ESI): calcd for $[M + Na]^+$ ($C_{24}H_{18}N_3O_2{}^{79}BrNaS$) = 514.0195; found: 514.0200.

3-((*E*)-(((*Z*)-4-([1,1′-Biphenyl]-3-yl)-3-benzylthiazol-2(3*H*)-ylidene)hydrazono)methyl)benzoic acid hydrobromide 22h. The product (205 mg, 90%) was obtained as a yellow solid. mp = 238 °C. ^{1}H NMR (300 MHz, DMSO-d_6) δ 8.36 (s, 1H), 8.30 (t, $^4J_{H-H}$ = 1.7 Hz, 1H), 7.94 (dd, $^3J_{H-H}$ = 7.5, $^4J_{H-H}$ = 1.7 Hz, 2H), 7.73 (dt, $^3J_{H-H}$ = 7.8, $^4J_{H-H}$ = 1.4 Hz, 1H), 7.61–7.19 (m, 12H), 7.11–7.00 (m, 2H), 6.72 (s, 1H), 5.16 (s, 2H). ^{13}C NMR (75 MHz, DMSO-d_6) δ 170.3, 167.2, 150.1, 140.6, 140.5, 139.1, 136.6, 135.4, 131.4, 131.3, 130.7, 130.3, 129.6, 129.3, 129.1, 128.8, 128.0, 128.0, 127.8, 127.5, 127.4, 127.1, 126.8, 126.3, 102.6, 49.0. HRMS (ESI): calcd for $[M + Na]^+$ ($C_{30}H_{23}N_3O_2NaS$) = 512.1409; found: 512.1409.

3-((*E*)-(((*Z*)-3-Benzyl-4-(3-benzylphenyl)thiazol-2(3*H*)-ylidene)hydrazono)methyl)benzoic acid hydrobromide 22i. The product (185 mg, 79%) was obtained as a yellow solid. mp = 221 °C. ^{1}H NMR (300 MHz, DMSO-d_6) δ 8.41 (s, 1H), 8.31 (t, $^4J_{H-H}$ = 1.7 Hz, 1H), 8.01–7.91 (m, 2H), 7.56 (t, $^3J_{H-H}$ = 7.7 Hz, 1H), 7.40–7.06 (m, 12H), 6.99–6.89 (m, 2H), 6.70 (s, 1H), 5.14 (s, 2H), 3.87 (s, 2H). ^{13}C NMR (75 MHz, DMSO-d_6) δ 170.0, 167.0, 150.0, 141.9, 140.8, 136.0, 135.0, 131.4, 131.3, 130.4, 129.9, 129.9, 129.3, 129.2, 128.9, 128.6, 128.6, 128.5, 127.6, 127.4, 127.3, 126.7, 126.3, 126.1, 103.0, 48.9, 40.8. HRMS (ESI): calcd for $[M + Na]^+$ ($C_{31}H_{26}N_3O_2NaS$) = 504.1740; found: 504.1736.

3-((*E*)-(((*Z*)-3-Benzyl-4-(3-phenoxyphenyl)thiazol-2(3*H*)-ylidene)hydrazono)methyl)benzoic acid hydrobromide 22j. The product (124 mg, 53%) was obtained as a yellow solid. mp = 215 °C. ^{1}H NMR (300 MHz, DMSO-d_6) δ 8.39 (s, 1H), 8.30 (t, $^4J_{H-H}$ = 1.8 Hz, 1H), 7.99–7.90 (m, 2H), 7.56 (t, $^3J_{H-H}$ = 7.7 Hz, 1H), 7.43 (t, $^3J_{H-H}$ = 7.9 Hz, 1H), 7.36 (t, $^3J_{H-H}$ = 7.9 Hz, 2H), 7.31–7.20 (m, 3H), 7.19–7.02 (m, 3H), 7.01–6.85 (m, 5H), 6.72 (s, 1H), 5.16 (s, 2H). ^{13}C NMR (75 MHz, DMSO-d_6) δ 170.0, 167.0, 156.7, 156.1, 150.0, 139.8, 136.1, 135.1, 131.6, 131.4, 131.2, 130.5, 130.3, 130.1, 129.2, 128.6, 127.5, 127.4, 126.3, 124.0, 123.8, 119.6, 118.9, 118.7, 103.2, 48.8. HRMS (ESI): calcd for $[M + Na]^+$ ($C_{30}H_{23}N_3O_3NaS$) = 528.1352; found: 528.1348.

3-((*E*)-(((*Z*)-3-Benzyl-4-(2-phenoxyphenyl)thiazol-2(3*H*)-ylidene)hydrazono)methyl)benzoic acid hydrobromide 22k. The product (145 mg, 62%) was obtained as a yellow solid. mp = 228 °C. ^{1}H NMR (300 MHz, DMSO-d_6) δ 8.35 (s, 1H), 8.27 (s, 1H), 7.92 (t, $^3J_{H-H}$ = 6.6 Hz, 2H), 7.64–6.80 (m, 15H), 6.63 (s, 1H), 5.12 (s, 2H). ^{13}C NMR (75 MHz, DMSO-d_6) δ 169.6, 167.1, 155.7, 155.1, 149.8, 136.6, 136.1, 135.2, 132.5, 132.0, 131.4, 131.3, 130.3, 130.2, 129.3, 128.6, 127.5, 127.5, 126.7, 124.3, 123.6, 120.9, 119.1, 118.0, 103.9, 48.6. HRMS (ESI): calcd for $[M + Na]^+$ ($C_{30}H_{24}N_3O_3S$) = 506.1533; found: 506.1536.

3-((*E*)-(((*Z*)-3-Benzyl-4-(2-(*p*-tolyloxy)phenyl)thiazol-2(3*H*)-ylidene)hydrazono)methyl)benzoic acid hydrobromide 22l. The product (180 mg, 75%) was obtained as a yellow solid. mp = 212 °C. ^{1}H NMR (300 MHz, DMSO-d_6) δ 8.31 (s, 1H), 8.25 (t, $^4J_{H-H}$ = 1.8 Hz, 1H), 7.92 (dt, $^3J_{H-H}$ = 7.9, $^4J_{H-H}$ = 1.5 Hz, 1H), 7.87 (dt, $^3J_{H-H}$ = 7.9, $^4J_{H-H}$ = 1.5 Hz, 1H), 7.52 (t, $^3J_{H-H}$ = 7.8 Hz, 1H), 7.38 (td, $^3J_{H-H}$ = 7.8, $^4J_{H-H}$ = 1.8 Hz, 1H), 7.28–7.15 (m, 4H), 7.12 (d, $^3J_{H-H}$ = 8.3 Hz, 2H), 7.06 (t, $^3J_{H-H}$ = 7.5 Hz, 1H), 6.98–6.91 (m, 2H), 6.81–6.71 (m, 3H), 6.63 (s, 1H), 5.10 (s, 2H), 2.22 (s, 3H). ^{13}C NMR (75 MHz, DMSO-d_6) δ 169.9, 167.5, 155.9, 153.4, 150.1, 137.2, 136.1, 135.3, 133.9, 132.7, 132.3, 131.7, 131.7, 130.9, 130.8, 129.6, 128.9, 127.9, 127.8, 126.9, 123.5, 120.6, 119.6, 117.5, 104.6, 49.0, 20.7. HRMS (ESI): calcd for $[M + H]^+$ ($C_{31}H_{26}N_3O_3S$) = 520.1689; found: 520.1686.

3-((*E*)-(((*Z*)-3-Benzyl-4-(2-(*o*-tolyloxy)phenyl)thiazol-2(3*H*)-ylidene)hydrazono)methyl)benzoic acid hydrobromide 22m. The product (165 mg, 69%) was obtained as a yellow solid. mp = 213 °C. ^{1}H NMR (300 MHz, DMSO-d_6) δ 8.29 (s, 1H), 8.25 (t, $^4J_{H-H}$ = 1.7 Hz, 1H), 7.89 (ddt, $^3J_{H-H}$ = 9.8 Hz, $^3J_{H-H}$ = 8.0 Hz, $^4J_{H-H}$ = 1.4 Hz, 2H), 7.53 (t, $^3J_{H-H}$ = 7.7 Hz, 1H), 7.39 (ddd, $^3J_{H-H}$ = 8.4 Hz, $^3J_{H-H}$ = 7.4 Hz, $^4J_{H-H}$ = 1.7 Hz, 1H), 7.33–7.24 (m, 2H), 7.24–7.13 (m, 4H), 7.07 (tt, $^3J_{H-H}$ = 7.4 Hz, $^4J_{H-H}$ = 1.2 Hz, 2H), 7.00–6.94 (m, 2H), 6.72 (dd, $^3J_{H-H}$ = 8.0, $^3J_{H-H}$ = 1.3 Hz, 1H), 6.66 (dd, $^3J_{H-H}$ = 8.3 Hz, $^4J_{H-H}$ = 1.0 Hz, 1H), 6.55 (s, 1H), 5.09 (s, 2H), 2.07 (s, 3H). ^{13}C NMR (75 MHz, DMSO-d_6) δ 170.1, 167.5, 155.5, 153.6, 150.0, 136.8, 136.5, 135.6, 132.7, 132.2, 132.0, 131.7, 131.6, 130.6, 129.6, 129.4, 128.9, 128.0, 127.8, 127.7, 126.9, 125.0, 123.4, 120.5, 119.6, 116.8, 103.5, 48.7, 16.0. HRMS (ESI): calcd for $[M + H]^+$ ($C_{31}H_{26}N_3O_3S$) = 520.1689; found: 520.1687.

3-((*E*)-(((*Z*)-3-Benzyl-4-(2-(*m*-tolyloxy)phenyl)thiazol-2(3*H*)-ylidene)hydrazono)methyl)benzoic acid hydrobromide 22n. The product (163 mg, 68%) was obtained as a yellow solid. mp = 201 °C. ^{1}H NMR (300 MHz, DMSO-d_6) δ 8.28 (s, 1H), 8.25 (t, $^4J_{H-H}$ = 1.7 Hz, 1H), 7.91 (dt, $^3J_{H-H}$ = 7.8 Hz, $^4J_{H-H}$ = 1.6 Hz, 1H),

7.87 (dt, $^3J_{H-H}$ = 7.8 Hz, $^3J_{H-H}$ = 1.3 Hz, 1H), 7.52 (t, $^4J_{H-H}$ = 7.7 Hz, 1H), 7.48–7.36 (m, 1H), 7.30–7.17 (m, 5H), 7.10 (td, $^4J_{H-H}$ = 7.5 Hz, $^4J_{H-H}$ = 1.1 Hz, 1H), 6.99–6.89 (m, 3H), 6.84 (dd, $^4J_{H-H}$ = 8.3 Hz, $^4J_{H-H}$ = 1.1 Hz, 1H), 6.71–6.63 (m, 2H), 6.53 (s, 1H), 5.06 (s, 2H), 2.22 (s, 3H). ^{13}C NMR (75 MHz, DMSO-d_6) δ 170.1, 167.5, 155.8, 155.4, 150.0, 140.4, 136.9, 136.5, 135.6, 132.7, 132.2, 131.7, 131.6, 130.6, 130.2, 129.6, 128.9, 127.8, 127.6, 126.9, 125.3, 123.8, 121.2, 119.9, 118.1, 116.4, 103.7, 48.7, 21.2. HRMS (ESI): calcd for $[M + H]^+$ ($C_{31}H_{26}N_3O_3S$) = 520.1689; found: 520.1691.

3-((*E*)-(((*Z*)-4-(3-Bromophenyl)-3-(pyridin-3-ylmethyl)thiazol-2(3*H*)-ylidene)hydrazono)methyl)benzoic acid hydrobromide 23e. The product (117 mg, 51%) was obtained as a yellow solid. mp = 238 °C. ^{1}H NMR (300 MHz, methanol-d_4) δ 8.79 (d, $^3J_{H-H}$ = 5.7 Hz, 1H), 8.72 (d, $^4J_{H-H}$ = 2.0 Hz, 1H), 8.38 (dt, $^3J_{H-H}$ = 8.3, $^4J_{H-H}$ = 1.7 Hz, 1H), 8.35 (t, $^4J_{H-H}$ = 1.7 Hz, 1H), 8.31 (s, 1H), 8.10–8.00 (m, 2H), 7.95 (d, $^3J_{H-H}$ = 8.0 Hz, 1H), 7.74–7.61 (m, 1H), 7.55 (s, 1H), 7.52 (t, $^3J_{H-H}$ = 8.0 Hz, 1H), 7.44–7.36 (m, 2H), 6.52 (s, 1H), 5.31 (s, 2H). ^{13}C NMR (75 MHz, methanol-d_4) δ 171.7, 169.3, 152.7, 146.4, 142.3, 142.2, 139.8, 139.0, 136.9, 134.1, 133.5, 133.3, 132.6, 132.4, 132.1, 131.9, 130.0, 129.5, 129.3, 128.6, 123.9, 104.6, 47.4. HRMS (ESI): calcd for $[M - H]^-$ ($C_{23}H_{16}N_4O_2{}^{79}BrS$) = 491.0182; found: 491.0181.

3-((*E*)-(((*Z*)-3-Benzyl-5-methyl-4-(3-phenoxyphenyl)thiazol-2(3*H*)-ylidene)hydrazono)methyl)benzoic acid hydrobromide 24j. The product (204 mg, 85%) was obtained as a yellow solid. mp = 258 °C. ^{1}H NMR (300 MHz, DMSO-d_6) δ 8.37 (s, 1H), 8.30 (t, $^4J_{H-H}$ = 1.4 Hz, 1H), 7.93 (tt, $^3J_{H-H}$ = 9.0, $^4J_{H-H}$ = 1.4 Hz, 2H), 7.55 (t, $^3J_{H-H}$ = 7.7 Hz, 1H), 7.48–7.42 (t, $^3J_{H-H}$ = 7.7 Hz, 1H), 7.39–7.32 (m, 2H), 7.29–7.17 (m, 3H), 7.16–7.13 (m, 1H), 7.12–7.04 (m, 2H), 6.98–6.90 (m, 2H), 6.90–6.84 (m, 2H), 6.76 (t, J = 2.0 Hz, 1H), 5.04 (s, 2H), 2.02 (s, 3H). ^{13}C NMR (75 MHz, DMSO-d_6) δ 168.4, 167.1, 156.8, 156.2, 149.6, 135.9, 135.1, 134.8, 131.5, 130.7, 130.4, 130.4, 130.2, 129.3, 128.7, 127.5, 127.4, 126.4, 125.4, 123.9, 120.2, 119.8, 118.9, 118.8, 113.7, 49.1, 12.3. HRMS (ESI): calcd for $[M + Na]^+$ ($C_{31}H_{25}N_3O_3NaS$) = 542.1508; found: 542.1505.

– Biological studies

Cell culture

The IGROV1-R10 cell line was established as described previously[49] from the IGROV1 cell line, which was kindly provided by Dr Jean Bénard (Institut Gustave Roussy, Paris, France). Cells were grown in RPMI 1640 (Gibco, 72400) medium supplemented with 2 mM Glutamax™, 25 mM HEPES (4-(2-hydroxyethyl)-1-piperazineethanesulfonic acid), 10% decomplemented FBS (fetal bovine serum) (Gibco, 10270106) and 33 mM sodium bicarbonate (Gibco, 25080094) and were maintained under a 5% CO_2 humidified atmosphere at 37 °C. This cell line was certified mycoplasma-free using MycoAlert® Mycoplasma Detection Kits (Lonza, LT07-318).

Chemicals

MIM1 analogs were synthesized in our laboratory as described above. ABT-737 (Bcl-x_L inhibitor) and S63845 (Mcl-1 inhibitor) were obtained from Selleckchem and Chemietek, respectively. Dimethyl sulfoxide (DMSO) was obtained from Sigma-Aldrich. The compounds were commonly stored as stock solutions in DMSO at −20 °C.

siRNA synthesis and transfection

All siRNAs used in these studies were chemically synthesized (Eurogentec) and received as annealed oligonucleotides. Sequences were as follows: siBcl-x_L (targeting specifically the Bcl-x_L mRNA but not the Bcl-x_S mRNA): sense sequence of the siRNA directed against Bcl-x_L is 5′-auuggugagucggaucgcatt-3′ and antisense sequence is 5′-ugcgauccgacucaccaautt-3′; siMcl-1: sense sequence of the siRNA directed against Mcl-1 is 5′-gug ccuuuguggcuaaacatt-3′ and antisense sequence is 5′-uguuua gccacaaaggcactt-3′. The sequence of the siControl (noted siCtl) has no sequence homology with any known genes in the human genome. Its sense sequence is 5′-gacguaaacggccac aagutt-3′ and its antisense sequence is 5′-acuuggccguuuacg uctt-3′. Transfection was performed on exponentially growing cells seeded the day before to reach 30–50% confluency at the time of transfection, according to the manufacturer's instructions. Briefly, the transfecting INTERFERin™ reagent (Polyplus Transfection) was added to siRNA (final concentration: 20 nM) diluted in Opti-MEM reduced serum medium (Gibco) and complex formation was allowed to proceed for 15 min at room temperature before being applied to cells. The following day, the cell media was changed to remove the transfecting reagent.

Real-time caspase 3/7 activation assay using time-lapse imaging

Caspase-3/7 activation was assessed using the IncuCyte caspase-3/7 green apoptosis assay reagent (Sartorius) as described previously.[50] Briefly, 7000 IGROV1-R10 cells per microwell were seeded in 96-well plates. After 24 h, cells were exposed to treatments and caspase 3/7 reagent was added at a final concentration of 5 mM (Sartorius). Real-time fluorescent images were acquired using IncuCyte S3 (Sartorius) every hour in two separate regions per well using a 10× objective. The IncuCyte caspase3/7 green reagent labels apoptotic cells, yielding green fluorescence. The live-cell phase contrast images were used to calculate confluence using the IncuCyte® software and to provide morphology information. Accumulation of IncuCyte caspase3/7 green over time was normalized to the confluence of cells. Each condition was performed in triplicate and averages with SD at each time point were plotted in Excel.

Real-time cell activity

A total of 7000 IGROV1-R10 cells per well were plated in a 96-well E-Plate view and were placed onto the xCELLigence real-time cell analysis (RTCA MP, Agilent) located inside a tissue culture incubator. Cells were grown for 24 hours before treatment and impedance was continuously measured until the end of the treatment. The impedance of each well was expressed as a cellular index (CI) value. SDs of well replicates were analyzed with the RTCA 2.1.0 Software.

Western blot analyses

Cells were rinsed with ice-cold PBS, suspended in a lysis buffer [RIPA: NaCl 150 mM, Tris (pH 8) 50 mM, Triton X100 1%, PMSF

4 mM, EDTA 5 mM, NaF 10 mM, NaPPi 10 mM, Na_3OV_4 1 mM, aprotinin 0.5 μL mL^{-1} and 4.6 mL ultra-pure water] and incubated on ice for 30 minutes. Lysates were collected after centrifugation (13 200*g*, 10 minutes, 4 °C) and protein concentrations were determined using the Bradford assay (Bio-Rad). 20 μg of proteins were prepared in ultrapure water in the presence of a loading buffer (laemmli + DTT (DiThioThreitol) [10%]) and heated at 100 °C for 10 minutes. Then the samples were separated by SDS-PAGE on a 4–15% gradient polyacrylamide gel (Bio-Rad) and transferred to PVDF membranes (Bio-Rad). After blocking non-specific binding sites for 1 hour at room temperature using 5% (w/v) non-fat dry milk in TBS with 0.5% (v/v) Tween20 (T-TBS), the membranes were incubated overnight at 4 °C with the following rabbit monoclonal antibodies: caspase 3 (cell signaling technology, 9662S), cleaved caspase 3 (cell signaling technology, 9661S), PARP (cell signaling technology, 9542S) or mouse monoclonal antibody: tubulin (Sigma-Aldrich, T6199). Membranes were then washed with T-TBS and incubated for 1 hour with the appropriate horseradish peroxidase-conjugated anti-rabbit (cell signaling technology, 7074S) or anti-mouse (Amersham, NA931V) secondary antibodies. Immune complexes were revealed using an ECL solution (Enhanced ChemiLuminescence, Clarity & Clarity Max, Bio-Rad) and were acquired using a luminescence image analyzer (GE Healthcare). Quantification was performed using the ImageQuantTL software.

Nuclei staining by DAPI

After treatment, both detached and adherent cells were pooled after trypsinization, applied to a polylysine-coated glass slide by cytocentrifugation and fixed with a solution of ethanol/chloroform/acetic acid (6 : 3 : 1). The preparations were then incubated for 15 min at room temperature with 1 μg mL^{-1} DAPI solution (Boehringer Mannheim-Roche), washed in distilled water, mounted under a coverslip in Mowiol (Calbiochem, 475904) and analyzed under a fluorescence microscope (VS120, Olympus).

DNA content analysis by flow cytometry

Adherent and floating cells were pooled, washed with 1× PBS and fixed with ethanol 70%. Before flow cytometry analysis, cells were centrifuged at 400*g* for 5 min and incubated for 30 min at 37 °C in PBS to allow the release of low-molecular-weight DNA (characteristic of apoptotic cells). Cell pellets were stained with propidium iodide (PI) using the DNA Prep Coulter Reagent Kit (Beckman-Coulter, 6607055). Samples were thereafter analyzed using a Gallios flow cytometer (Beckman Coulter) and cell cycle distribution was determined using Kaluza acquisition software (Beckman Coulter).

– Molecular modelling studies

For these studies, the material and methods were identical to those described in a previous paper.[44]

Discussion

In this publication, we evaluated the impact of a major chemical variation (replacement of triphenol with an acid) on previously described compounds[44] in a cell model relevant for identifying potential inhibitors of Bcl-x_L and/or Mcl-1. The IGROV1-R10 ovarian cancer cell line was specifically chosen for its well-characterized, dual dependency on both Mcl-1 and Bcl-x_L for survival, offering a robust and mechanistically informative platform for functional screening. We first designed a strategy that allowed us to fully control, on the thiazole unit, the nature of the substituents $\mathbf{R^1}$ and $\mathbf{R^2}$ required for the structure–activity studies. Then we evaluated the capacity of the newly synthesized compounds to induce apoptosis in combination with siRNAs or pharmacological inhibitors of Bcl-x_L or Mcl-1, as described above, in order to identify potential inhibitors of Bcl-x_L, Mcl-1 or both. In the first screening phase, we used siRNA-mediated silencing of Mcl-1 and Bcl-x_L in IGROV1-R10 cells to create a controlled and specific sensitization context. siRNA was indeed preferred for a screening setup at this stage due to its high specificity and reproducibility. In subsequent validation, we transitioned to using pharmacological inhibitors (S63845 for Mcl-1 and ABT-737 for Bcl-x_L). This was done to mimic potential therapeutic conditions more closely and to facilitate dose-dependent, reversible inhibition that better reflects clinical application. As the IGROV1-R10 cell line relies on both Mcl-1 and Bcl-x_L for survival, monotherapy with Mcl-1 inhibitors, including our compounds, does not induce measurable cytotoxicity, thereby precluding the determination of conventional IC_{50} values in this model. Biological activity was therefore assessed at fixed concentrations (10 and 25 μM), based on our previous structure–activity relationship (SAR) studies on MIM1 derivatives,[44,45] and in line with concentrations used in other published studies assessing MIM1,[51,52] which typically range between 1 and 50 μM. One Mcl-1 inhibitor was identified (compound **22a**) in the first series and a second in the second series (compound **22k**). In the third series, compounds **22l**, **22m** and **22n** showed modest activity as Mcl-1 inhibitors, with optimal activity for **22l**. However, while the proportions of events in the sub-G1 fraction on the DNA content histograms appear to be similar to the results obtained for molecules **22a** and **22k**, the cellular and nuclear morphologies show very significant differences, suggesting that these molecules are far less active than molecules **22a** and **22k**, as also suggested by the level of cleaved PARP and caspase 3 on western blots. Thus, **22a** and **22k** compounds constitute the hits of these series. Interestingly, no Bcl-x_L inhibitors were identified, although a slight effect of the **22n** compound could be suggested by the observation of sub-G1 events and low levels of cleaved PARP and caspase 3 bands when this compound was associated with S63845. It should be noted that flow cytometry provides qualitative information on cell viability, but its quantitative nature is unreliable, particularly in the presence of cells in advanced apoptosis. Indeed, since the nuclei of these cells are likely to fragment and lead to the formation of multiple apoptotic bodies, a single nucleus is thus capable of leading to the observation of multiple events in the sub-G1 fraction, resulting in an overestimation of the proportion of cells in apoptosis. Accompanying these results with the observation of cell and nuclear morphologies is thus

essential and assessment of the proportion of cleaved PARP and cleaved caspase 3 on western blot can usefully complement this information in a semi-quantitative way. While no direct binding assay was performed here, the compounds tested belong to a series of MIM1 derivatives whose interaction with Mcl-1 has been previously confirmed by fluorescence polarization assays.[43–45] In our IGROV1-R10 model, which exhibits dual dependency on Bcl-x_L and Mcl-1, these compounds did not induce apoptosis when used alone or with a potent Mcl-1 inhibitor (S63845), but showed strong apoptotic activity when combined with a Bcl-x_L inhibitor. This behavior is highly indicative of Mcl-1 inhibition and supports the proposed mechanism of action. Further mechanistic studies will be needed to validate these findings fully.

In the past few years, various inhibitors have been developed and some of them have been the subject of clinical trials in recent years, not only for hematological malignancies, but also for solid tumors.[53] Among the clinical-stage Mcl-1 inhibitors, AMG-176 and AZD5991 showed submicromolar potency in sensitive cell lines.[54,55] In our IGROV1-R10 model, both compounds induced massive apoptosis when combined with ABT-737, at concentrations of 1 μM and 0.5 μM, respectively (data not shown). Unlike these extensively optimized compounds, our study focuses on early-stage hit molecules, identified through a functional screen and showing activities in the 10–25 μM range. At this stage, our primary objective was not to achieve maximal potency, but rather to uncover promising scaffolds for further development.

However, it should be mentioned that these clinical trials have highlighted some toxicities: significant thrombocytopenia has been linked to Bcl-x_L inhibition,[56] while Mcl-1 inhibition strategies led to cardiac toxicity.[57,58] These limitations of direct Mcl-1 or Bcl-x_L inhibition have led to increasing interest in alternative strategies such as PROTACs (proteolysis-targeting chimeras). These molecules promote targeted degradation of Mcl-1[59,60] or Bcl-x_L[61] and may offer safer therapeutic profiles, as illustrated by the absence of thrombocytopenia typically associated with Bcl-x_L inhibition, such as that seen with Navitoclax.[62–65] Indeed, a key advantage of PROTACs is the possibility to modulate tissue distribution and reduce systemic exposure, particularly to cardiac tissue, by exploiting the tissue-specific expression of E3 ligases or through cell-selective delivery strategies. In this context, high-affinity binding is not always required. Even moderate-affinity ligands can serve as effective warheads, provided they allow for stable ternary complex formation. Additionally, ligands that bind to non-functional or allosteric sites, while not inhibitory *per se*, can still be highly valuable if they enable efficient recruitment of Mcl-1 to the ubiquitin-proteasome system.[66] Future development of our compounds could benefit from such approaches.

Finally, once more advanced and optimized compounds are available, future work will include expanding biological evaluations to additional cancer models to assess both selectivity and broader therapeutic potential. Evaluation of off-target effects, particularly in non-cancerous and physiologically relevant systems, will also be an important step to better characterize the safety profile of these compounds.

Conclusion

We have designed and prepared new heterocyclic derivatives ''inspired'' from MIM1, a known selective inhibitor of the Mcl-1 anti-apoptotic protein. For these novel compounds, we have successfully replaced the triphenol core of MIM1 with a benzoic acid entity, designed to keep the key anchoring of these derivatives to the important amino acids R263 of Mcl-1 and to introduce appropriate aromatic groups in the lipophilic pocket. These studies led to two new interesting molecules, **22a** and **22k**, which are potent and selective inhibitors of Mcl-1. Extensive molecular modelling studies have been performed to rationalize these results. Together, these results show that it is possible to replace the trisphenol structure of MIM1 with an acid in the *meta*-position and to obtain good inhibitors of Mcl-1. Moreover, this isosteric replacement brings a strong selectivity towards Bcl-x_L. The structure–activity relationships we presented here also showed that a given chemical scaffold is prone to reorientation, or even to switch completely in a binding site as shallow and exposed as that of Mcl-1. This makes predicting scaffold optimization particularly difficult. Together, these results confirm that it is possible to design small and relatively simple molecules with potent activities, in ovarian cancer cell lines, against the Mcl-1 anti-apoptotic protein. Since Mcl-1 could be a pertinent target in various hematological and solid malignancies, the design of potent molecules and/or of their PROTAC derivatives must continue to be the focus of new investigations.

Conflicts of interest

The authors declare no conflict of interest.

Data availability

Data are available upon request from the authors. The data supporting this article have been included in the ESI.† Sample of the compounds are available from the authors.

Acknowledgements

This research was supported by the Research Grant program at Lebanese University, Lebanon. The authors would like to acknowledge the National Council for Scientific Research of Lebanon (CNRS-L), Agence Universitaire de la Francophonie (AUF), and the Lebanese University (UL) for granting a doctoral fellowship to Ali Soulieman. We also thank the University of Rennes and CNRS (UMR 6226) for their financial support. We thank Pr J. Boustie for fruitful discussions and constant support. We are very grateful to the Centre Régional de Mesures Physiques de l'Ouest, Rennes (CRMPO) team for the physicochemical analyses. Financial support by the ''Ligue contre le

Cancer, Conseil Interrégional Grand Ouest'' and ''Ligue Contre le Cancer, Conseil Interrégional de Normandie et Comité du Calvados'' is gratefully acknowledged. This work was also supported by the ''Conseil Régional de Normandie'' and the European Union (PLATONUS ONE and Equip'Innov Caen 2022 – Sub project PLATONUS-ONE projects supported by the Normandy County Council and the European Union within the framework of the Operational Programme ERDF/ESF 2014–2020) and by the French State (CPER Innovons 2), the University of Caen Normandie and Inserm. H. P. is recipient of a doctoral fellowship from the ''Ministère de l'Enseignement Supérieur, de la Recherche et de l'Innovation'' granted by Normandy Doctoral School 497 ''EDN Bise''. We acknowledge Maryline Guillamin (IsoCELL cytometry core facility from PLATON Services Unit, University of Caen Normandie, for her helpful technical support and Pr Roman Rouzier, head of the Comprehensive Cancer Center François Baclesse (Caen, France), for his constant support. J. P. and H. P. were recipients of doctoral scholarships from the French ministry of research and higher education.

References

1 D. Hanahan, *Cancer Discovery*, 2022, **12**, 31–46.
2 P. E. Czabotar, G. Lessene, A. Strasser and J. M. Adams, *Nat. Rev. Mol. Cell Biol.*, 2014, **15**, 49–63.
3 J. M. Adams and S. Cory, *Cell Death Differ.*, 2018, **25**, 27–36.
4 A. R. D. Delbridge and A. Strasser, *Cell Death Differ.*, 2015, **22**, 1071–1080.
5 H.-C. Zheng, *Oncotarget*, 2017, **8**, 59950–59964.
6 S. K. Tahir, X. Yang, M. G. Anderson, S. E. Morgan-Lappe, A. V. Sarthy, J. Chen, R. B. Warner, S.-C. Ng, S. W. Fesik, S. W. Elmore, S. H. Rosenberg and C. Tse, *Cancer Res.*, 2007, **67**, 1176–1183.
7 E. Wesarg, S. Hoffarth, R. Wiewrodt, M. Kröll, S. Biesterfeld, C. Huber and M. Schuler, *Int. J. Cancer*, 2007, **121**, 2387–2394.
8 K. E. Tagscherer, A. Fassl, B. Campos, M. Farhadi, A. Kraemer, B. C. Böck, S. Macher-Goeppinger, B. Radlwimmer, O. D. Wiestler, C. Herold-Mende and W. Roth, *Oncogene*, 2008, **27**, 6646–6656.
9 E. Brotin, M. Meryet-Figuière, K. Simonin, R. E. Duval, M. Villedieu, J. Leroy-Dudal, E. Saison-Behmoaras, P. Gauduchon, C. Denoyelle and L. Poulain, *Int. J. Cancer*, 2010, **126**, 885–895.
10 D. Kaloni, S. T. Diepstraten, A. Strasser and G. L. Kelly, *Apoptosis*, 2023, **28**, 20–38.
11 C. Gloaguen, A. S. Voisin-Chiret, J. Sopkova-de Oliveira Santos, J. Fogha, F. Gautier, M. De Giorgi, G. Burzicki, S. Perato, C. Pétigny-Lechartier, K. Simonin-Le Jeune, E. Brotin, D. Goux, M. N'Diaye, B. Lambert, M.-H. Louis, L. Ligat, F. Lopez, P. Juin, R. Bureau, S. Rault and L. Poulain, *J. Med. Chem.*, 2015, **58**, 1644–1668.
12 S. Hedir, M. De Giorgi, J. Fogha, M. De Pascale, L.-B. Weiswald, E. Brotin, B. Marekha, C. Denoyelle, C. Denis, P. Suzanne, F. Gautier, P. Juin, L. Ligat, F. Lopez, L. Carlier, R. Legay, R. Bureau, S. Rault, L. Poulain, J. S. Oliveira Santos and A. S. Voisin-Chiret, *Eur. J. Med. Chem.*, 2018, **159**, 357–380.
13 C. E. Weeden, C. Ah-Cann, A. Z. Holik, J. Pasquet, J.-M. Garnier, D. Merino, G. Lessene and M.-L. Asselin-Labat, *Oncogene*, 2018, **37**, 4475–4488.
14 E. F. Lee, T. J. Harris, S. Tran, M. Evangelista, S. Arulananda, T. John, C. Ramnac, C. Hobbs, H. Zhu, G. Gunasingh, D. Segal, A. Behren, J. Cebon, A. Dobrovic, J. M. Mariadason, A. Strasser, L. Rohrbeck, N. K. Haass, M. J. Herold and W. D. Fairlie, *Cell Death Dis.*, 2019, **10**, 342.
15 M. Hormi, R. Birsen, M. Belhadj, T. Huynh, L. Cantero Aguilar, E. Grignano, L. Haddaoui, F. Guillonneau, P. Mayeux, M. Hunault, J. Tamburini, O. Kosmider, M. Fontenay, D. Bouscary and N. Chapuis, *Eur. J. Haematol.*, 2020, **105**, 588–596.
16 K. Simonin, M. N'Diaye, S. Lheureux, C. Loussouarn, S. Dutoit, M. Briand, F. Giffard, E. Brotin, C. Blanc-Fournier and L. Poulain, *Apoptosis*, 2013, **18**, 492–508.
17 Z. Baranski, Y. de Jong, T. Ilkova, E. F. P. Peterse, A.-M. Cleton-Jansen, B. van de Water, P. C. W. Hogendoorn, J. V. M. G. Bovée and E. H. J. Danen, *Oncotarget*, 2015, **6**, 36113–36125.
18 A. Jebahi, M. Villedieu, C. Pétigny-Lechartier, E. Brotin, M.-H. Louis, E. Abeilard, F. Giffard, M. Guercio, M. Briand, P. Gauduchon, S. Lheureux and L. Poulain, *Cancer Lett.*, 2014, **348**, 38–49.
19 M.-L. Bonnefond, B. Lambert, F. Giffard, E. Abeilard, E. Brotin, M.-H. Louis, M. S. Gueye, P. Gauduchon, L. Poulain and M. N'Diaye, *Apoptosis*, 2015, **20**, 535–550.
20 C. Pétigny-Lechartier, C. Duboc, A. Jebahi, M.-H. Louis, E. Abeilard, C. Denoyelle, P. Gauduchon, L. Poulain and M. Villedieu, *Mol. Cancer Ther.*, 2017, **16**, 102–115.
21 M.-L. Bonnefond, R. Florent, S. Lenoir, B. Lambert, E. Abeilard, F. Giffard, M.-H. Louis, N. Elie, M. Briand, D. Vivien, L. Poulain, P. Gauduchon and M. N'Diaye, *Oncotarget*, 2018, **9**, 33896–33911.
22 C. Alcon, F. Martín, E. Prada, J. Mora, A. Soriano, G. Guillén, S. Gallego, J. Roma, J. Samitier, A. Villanueva and J. Montero, *Cell Death Discovery*, 2022, **8**, 172.
23 J. Li, C.-H. Chen, K. L. O'Neill, V. J. Fousek-Schuller, A. R. Black, J. D. Black, J. Zhang and X. Luo, *J. Biol. Chem.*, 2023, **299**, 102875.
24 Y. J. Thus, M. F. M. De Rooij, N. Swier, R. L. Beijersbergen, J. E. J. Guikema, M.-J. Kersten, E. Eldering, S. T. Pals, A. P. Kater and M. Spaargaren, *Haematologica*, 2023, **108**, 797–810.
25 L. M. Juárez-Salcedo, V. Desai and S. Dalia, *Drugs Context*, 2019, **8**, 212574.
26 M. F. van Delft, A. H. Wei, K. D. Mason, C. J. Vandenberg, L. Chen, P. E. Czabotar, S. N. Willis, C. L. Scott, C. L. Day, S. Cory, J. M. Adams, A. W. Roberts and D. C. S. Huang, *Cancer Cell*, 2006, **10**, 389–399.
27 K. Simonin, E. Brotin, S. Dufort, S. Dutoit, D. Goux, M. N'diaye, C. Denoyelle, P. Gauduchon and L. Poulain, *Mol. Cancer Ther.*, 2009, **8**, 3162–3170.

28 P. Geserick, J. Wang, M. Feoktistova and M. Leverkus, *Cell Death Dis.*, 2014, **5**, e1412.
29 M. B. Vera, O. Morris-Hanon, G. I. Nogueiras, L. B. Ripari, M. I. Esquivel, C. Perez-Castro, L. Romorini, G. E. Sevlever, M. E. Scassa and G. A. Videla-Richardson, *Sci. Rep.*, 2022, **12**, 17729.
30 K. M. Lucas, N. Mohana-Kumaran, D. Lau, X. D. Zhang, P. Hersey, D. C. Huang, W. Weninger, N. K. Haass and J. D. Allen, *Clin. Cancer Res.*, 2012, **18**, 783–795.
31 A. R. Mattoo, J. Zhang, L. A. Espinoza and J. M. Jessup, *Clin. Cancer Res.*, 2014, **20**, 5446–5455.
32 E. Shang, T. T. T. Nguyen, C. Shu, M.-A. Westhoff, G. Karpel-Massler and M. D. Siegelin, *Cancers*, 2020, **12**, 2137.
33 S. Hedir, M. De Giorgi, J. Fogha, M. De Pascale, L.-B. Weiswald, E. Brotin, B. Marekha, C. Denoyelle, C. Denis, P. Suzanne, F. Gautier, P. Juin, L. Ligat, F. Lopez, L. Carlier, R. Legay, R. Bureau, S. Rault, L. Poulain, J. S. Oliveira Santos and A. S. Voisin-Chiret, *Eur. J. Med. Chem.*, 2018, **159**, 357–380.
34 M. Hormi, R. Birsen, M. Belhadj, T. Huynh, L. Cantero Aguilar, E. Grignano, L. Haddaoui, F. Guillonneau, P. Mayeux, M. Hunault, J. Tamburini, O. Kosmider, M. Fontenay, D. Bouscary and N. Chapuis, *Eur. J. Haematol.*, 2020, **105**, 588–596.
35 R. Beroukhim, C. H. Mermel, D. Porter, G. Wei, S. Raychaudhuri, J. Donovan, J. Barretina, J. S. Boehm, J. Dobson, M. Urashima, K. T. Mc Henry, R. M. Pinchback, A. H. Ligon, Y.-J. Cho, L. Haery, H. Greulich, M. Reich, W. Winckler, M. S. Lawrence, B. A. Weir, K. E. Tanaka, D. Y. Chiang, A. J. Bass, A. Loo, C. Hoffman, J. Prensner, T. Liefeld, Q. Gao, D. Yecies, S. Signoretti, E. Maher, F. J. Kaye, H. Sasaki, J. E. Tepper, J. A. Fletcher, J. Tabernero, J. Baselga, M.-S. Tsao, F. Demichelis, M. A. Rubin, P. A. Janne, M. J. Daly, C. Nucera, R. L. Levine, B. L. Ebert, S. Gabriel, A. K. Rustgi, C. R. Antonescu, M. Ladanyi, A. Letai, L. A. Garraway, M. Loda, D. G. Beer, L. D. True, A. Okamoto, S. L. Pomeroy, S. Singer, T. R. Golub, E. S. Lander, G. Getz, W. R. Sellers and M. Meyerson, *Nature*, 2010, **463**, 899–905.
36 A. H. Wei, A. W. Roberts, A. Spencer, A. S. Rosenberg, D. Siegel, R. B. Walter, S. Caenepeel, P. Hughes, Z. McIver, K. Mezzi, P. K. Morrow and A. Stein, *Blood Rev.*, 2020, **44**, 100672.
37 L. Song, D. Coppola, S. Livingston, D. Cress and E. B. Haura, *Cancer Biol. Ther.*, 2005, **4**, 267–276.
38 Q. Ding, X. He, W. Xia, J.-M. Hsu, C.-T. Chen, L.-Y. Li, D.-F. Lee, J.-Y. Yang, X. Xie, J.-C. Liu and M.-C. Hung, *Cancer Res.*, 2007, **67**, 4564–4571.
39 M. Krajewska, S. Krajewski, J. I. Epstein, A. Shabaik, J. Sauvageot, K. Song, S. Kitada and J. C. Reed, *Am. J. Pathol.*, 1996, **148**, 1567–1576.
40 Y. Miyamoto, R. Hosotani, M. Wada, J. U. Lee, T. Koshiba, K. Fujimoto, S. Tsuji, S. Nakajima, R. Doi, M. Kato, Y. Shimada and M. Imamura, *Oncology*, 1999, **56**, 73–82.
41 K. Shigemasa, O. Katoh, Y. Shiroyama, S. Mihara, K. Mukai, N. Nagai and K. Ohama, *Jpn. J. Cancer Res.*, 2002, **93**, 542–550.
42 H. Deng, Y. Han, L. Liu, H. Zhang, D. Liu, J. Wen, M. Huang and L. Zhao, *J. Med. Chem.*, 2024, **67**, 5963–5998.
43 N. A. Cohen, M. L. Stewart, E. Gavathiotis, J. L. Tepper, S. R. Bruekner, B. Koss, J. T. Opferman and L. D. Walensky, *Chem. Biol.*, 2012, **19**, 1175–1186.
44 H. Paysant, S. Hedir, F. Justaud, L. B. Weiswald, A. N. El Dine, A. Soulieman, A. Hachem, N. Elie, E. Brotin, C. Denoyelle, J. Bignon, F. Roussi, M. Jouanne, O. Tasseau, T. Roisnel, A. S. Voisin-Chiret, R. Grée, N. Levoin and L. Poulain, *Org. Biomol. Chem.*, 2021, **19**, 8968–8987.
45 F. Justaud, H. Paysant, L. B. Weiswald, A. Jebahi, M. Jouanne, N. Elie, A. S. Voisin-Chiret, T. Roisnel, C. Orionne, N. Levoin, L. Poulain and R. Grée, *New J. Chem.*, 2022, **46**, 9119–9127.
46 J. B. Baell and G. A. Holloway, *J. Med. Chem.*, 2010, **53**, 2719–2740.
47 J. Witham, M. R. Valenti, A. K. De-Haven-Brandon, S. Vidot, S. A. Eccles, S. B. Kaye and A. Richardson, *Clin. Cancer Res.*, 2007, **13**, 7191–7198.
48 A. Kotschy, Z. Szlavik, J. Murray, J. Davidson, A. L. Maragno, G. Le Toumelin-Braizat, M. Chanrion, G. L. Kelly, J.-N. Gong, D. M. Moujalled, A. Bruno, M. Csekei, A. Paczal, Z. B. Szabo, S. Sipos, G. Radics, A. Proszenyak, B. Balint, L. Ondi, G. Blasko, A. Robertson, A. Surgenor, P. Dokurno, I. Chen, N. Matassova, J. Smith, C. Pedder, C. Graham, A. Studeny, G. Lysiak-Auvity, A.-M. Girard, F. Gravé, D. Segal, C. D. Riffkin, G. Pomilio, L. C. A. Galbraith, B. J. Aubrey, M. S. Brennan, M. J. Herold, C. Chang, G. Guasconi, N. Cauquil, F. Melchiore, N. Guigal-Stephan, B. Lockhart, F. Colland, J. A. Hickman, A. W. Roberts, D. C. S. Huang, A. H. Wei, A. Strasser, G. Lessene and O. Geneste, *Nature*, 2016, **538**, 477–482.
49 L. Poulain, H. Lincet, F. Duigou, E. Deslandes, F. Sichel, P. Gauduchon and C. Staedel, *Int. J. Cancer*, 1998, **78**, 454–463.
50 K. Artymovich and D. M. Appledorn, *Methods Mol. Biol.*, 2015, **1219**, 35–42.
51 M. Respondek, A. Beberok, J. Rok, Z. Rzepka, D. Wrześniok and E. Buszman, *Toxicol. In Vitro*, 2018, **53**, 126–135.
52 M. Respondek, A. Beberok, Z. Rzepka, J. Rok and D. Wrześniok, *Pathol. Oncol. Res.*, 2020, **26**, 1465–1474.
53 H. Deng, Y. Han, L. Liu, H. Zhang, D. Liu, J. Wen, M. Huang and L. Zhao, *J. Med. Chem.*, 2024, **67**, 5963–5998.
54 S. Caenepeel, S. P. Brown, B. Belmontes, G. Moody, K. S. Keegan, D. Chui, D. A. Whittington, X. Huang, L. Poppe, A. C. Cheng, M. Cardozo, J. Houze, Y. Li, B. Lucas, N. A. Paras, X. Wang, J. P. Taygerly, M. Vimolratana, M. Zancanella, L. Zhu, E. Cajulis, T. Osgood, J. Sun, L. Damon, R. K. Egan, P. Greninger, J. D. McClanaghan, J. Gong, D. Moujalled, G. Pomilio, P. Beltran, C. H. Benes, A. W. Roberts, D. C. Huang, A. Wei, J. Canon, A. Coxon and P. E. Hughes, *Cancer Discovery*, 2018, **12**, 1582–1597.
55 A. E. Tron, M. A. Belmonte, A. Adam, B. M. Aquila, L. H. Boise, E. Chiarparin, J. Cidado, K. J. Embrey, E. Gangl, F. D. Gibbons, G. P. Gregory, D. Hargreaves, J. A. Hendricks, J. W. Johannes, R. W. Johnstone, S. L. Kazmirski,

J. G. Kettle, M. L. Lamb, S. M. Matulis, A. K. Nooka, M. J. Packer, B. Peng, P. B. Rawlins, D. W. Robbins, A. G. Schuller, N. Su, W. Yang, Q. Ye, X. Zheng, J. P. Secrist, E. A. Clark, D. M. Wilson, S. E. Fawell and A. W. Hird, *Nat. Commun.*, 2018, **9**, 5341.

56 A. W. Roberts, J. F. Seymour, J. R. Brown, W. G. Wierda, T. J. Kipps, S. L. Khaw, D. A. Carney, S. Z. He, D. C. S. Huang, H. Xiong, Y. Cui, T. A. Busman, E. M. McKeegan, A. P. Krivoshik, S. H. Enschede and R. Humerickhouse, *J. Clin. Oncol.*, 2012, **30**, 488–496.

57 X. Wang, M. Bathina, J. Lynch, B. Koss, C. Calabrese, S. Frase, J. D. Schuetz, J. E. Rehg and J. T. Opferman, *Genes Dev.*, 2013, **27**, 1351–1364.

58 L. Guo, S. Eldridge, M. Furniss, J. Mussio and M. Davis, *Toxicol. Appl. Pharmacol.*, 2018, **360**, 88–98.

59 J. W. Papatzimas, E. Gorobets, R. Maity, M. I. Muniyat, J. L. MacCallum, P. Neri, N. J. Bahlis and D. J. Derksen, *J. Med. Chem.*, 2019, **62**, 5522–5540.

60 Z. Wang, N. He, Z. Guo, C. Niu, T. Song, Y. Guo, K. Cao, A. Wang, J. Zhu, X. Zhang and Z. Zhang, *J. Med. Chem.*, 2019, **62**, 8152–8163.

61 A. Negi and A. S. Voisin-Chiret, *ChemBioChem*, 2022, **23**, e202100689.

62 S. Khan, X. Zhang, D. Lv, Q. Zhang, Y. He, P. Zhang, X. Liu, D. Thummuri, Y. Yuan, J. S. Wiegand, J. Pei, W. Zhang, A. Sharma, C. R. McCurdy, V. M. Kuruvilla, N. Baran, A. A. Ferrando, Y.-M. Kim, A. Rogojina, P. J. Houghton, G. Huang, R. Hromas, M. Konopleva, G. Zheng and D. Zhou, *Nat. Med.*, 2019, **25**, 1938–1947.

63 X. Zhang, D. Thummuri, Y. He, X. Liu, P. Zhang, D. Zhou and G. Zheng, *Chem. Commun.*, 2019, **55**, 14765–14768.

64 X. Zhang, D. Thummuri, X. Liu, W. Hu, P. Zhang, S. Khan, Y. Yuan, D. Zhou and G. Zheng, *Eur. J. Med. Chem.*, 2020, **192**, 112186.

65 Y. He, X. Zhang, J. Chang, H.-N. Kim, P. Zhang, Y. Wang, S. Khan, X. Liu, X. Zhang, D. Lv, L. Song, W. Li, D. Thummuri, Y. Yuan, J. S. Wiegand, Y. T. Ortiz, V. Budamagunta, J. H. Elisseeff, J. Campisi, M. Almeida, G. Zheng and D. Zhou, *Nat. Commun.*, 2020, **11**, 1996.

66 N. Guedeney, M. Cornu, F. Schwalen, C. Kieffer and A. S. Voisin-Chiret, *Drug Discovery Today*, 2023, **28**, 1–14.